Engineering Strategies for Low-Cost and High-Power Density Aluminum-Ion Batteries

Xiaolong Xu, Kwan San Hui, Kwun Nam Hui, Jianxing Shen, Guowei Zhou, Jinhua Liu, Yucheng Sun

PII: S1385-8947(21)00973-6
DOI: https://doi.org/10.1016/j.cej.2021.129385
Reference: CEJ 129385

To appear in: *Chemical Engineering Journal*

Received Date: 6 December 2020
Revised Date: 10 March 2021
Accepted Date: 12 March 2021

Please cite this article as: X. Xu, K. San Hui, K. Nam Hui, J. Shen, G. Zhou, J. Liu, Y. Sun, Engineering Strategies for Low-Cost and High-Power Density Aluminum-Ion Batteries, *Chemical Engineering Journal* (2021), doi: https://doi.org/10.1016/j.cej.2021.129385

Engineering Strategies for Low-Cost and High-Power Density Aluminum-Ion Batteries

Xiaolong Xu[*abcd], Kwan San Hui[*c], Kwun Nam Hui[*d], Jianxing Shen[a], Guowei Zhou[b], Jinhua Liu[a] and Yucheng Sun[e]

[a] School of Materials Science and Engineering, Qilu University of Technology (Shandong Academy of Sciences), No. 3501, Daxue Road, Changqing District, Jinan, Shandong Province, People's Republic of China.

[b] Key Laboratory of Fine Chemicals in Universities of Shandong, School of Chemistry and Pharmaceutical Engineering, Qilu University of Technology (Shandong Academy of Sciences), No. 3501, Daxue Road, Changqing District, Jinan, Shandong Province, People's Republic of China.

[c] School of Engineering, Faculty of Science, University of East Anglia, Norwich, NR4 7TJ, UK.

[d] Joint Key Laboratory of the Ministry of Education, Institute of Applied Physics and Materials Engineering, University of Macau, Avenida da Universidade, Taipa, Macau SAR, People's Republic of China.

[e] Qingdao Xinzheng Lithium Industry Co., Ltd., No.1 Shiyuan Road, Jihongtan Street, Chengyang District, Qingdao, People's Republic of China.

*Corresponding authors: Xiaolong Xu (xlxu@qlu.edu.cn) , Kwan San Hui (k.hui@uea.ac.uk) and Kwun Nam Hui (bizhui@um.edu.mo)

Abstract: Aluminum-ion batteries (AIBs) for electrochemical energy storage technologies are relatively new research hotspots because of their advantages, such as high theoretical specific capacity, lightweightness, zero pollution, safety, inexpensive and rich resource. Especially, AIBs possess the potential to achieve ultrafast charge and discharge speed because of three-electron redox reactions, becoming the most promising candidate for high power density rechargeable batteries. However, several serious drawbacks, such as passive film formation, anode corrosion, and cathode selection and preparation, hinder the large-scale application of these systems. Here, we introduce the principles of AIBs and review the challenges and outlooks of AIBs from various perspectives, including anode design and protection, electrolyte exploitation and battery design, and cathode selection and preparation. We comprehensively discuss the acquisition of green and low-cost carbonaceous cathode materials with high electrochemical performance. Furthermore, several perspectives on potential research directions for the development of high-power density AIBs are proposed.

Keywords: Electrochemical energy storage; Aluminum-ion battery; High-power density; Challenge; Research direction; Low-cost carbonaceous cathode

1 Introduction

With the increase in demand for fast charging speed of energy storage devices and further requirements for the operating power of high-performance electric vehicles, the power density of energy storage devices has become the focus of improvement [1-4]. Supercapacitors have a high power density owing to the energy storage mechanism of charge adsorption [5, 6]. However, the short discharge time cannot meet the requirements of portable equipment and electric vehicles [7]. Aluminum-ion batteries (AIBs) are potential candidates for meeting the above requirements because of their rapid charge and discharge speed caused by three-electron redox reactions [8-10]. Moreover, compared with lithium, sodium, potassium, magnesium, calcium, and zinc, aluminum possesses the advantages of high theoretical specific capacity, lightweightness, zero pollution, safety, low cost, and rich resource, which make it practicable for electric vehicles and large-scale energy storage [11] [12, 13]. Therefore, rechargeable AIB research has become a new hotspot in the field of energy storage.

Various studies have centered on the high electrochemical performance of AIBs [14-16]. Lin et al. [8] developed an ultrafast rechargeable AIB, which exhibited a discharge voltage platform near 2.0 V and a discharge specific capacity of 70 mA h g^{-1} at 4 A g^{-1}, withstanding more than 7500 cycles without capacity decay. Wu et al. [2] reported a monolithic three-dimensional graphitic foam as a cathode for rechargeable AIBs, exhibiting a discharge capacity of 60 mA h g^{-1} at 12 A g^{-1} and stable cycling over 4000 cycles. Zhao et al. [17] designed two-dimensional WS_2 layered cathode for high-performance AIBs, displaying a reversible capacity of 86 mA h g^{-1} at 5 A g^{-1}.

These studies reflect the potential of AIBs as a high-power-density energy storage device. Subsequently, several reviews summarized the research progress and challenges of AIBs. In 2018, Zhang et al. [18] reported the challenges, status, and perspectives of non-aqueous AIBs and discussed the development of reliable non-aqueous AIBs. Das [19] reported graphene as a cathode material of choice for AIBs and highlighted the electrochemical performances, advantages, and challenges of graphene as cathode for AIB in conjugation with chloroaluminate-based electrolytes. In 2019, Verma et al. [20] reported the progress in rechargeable aqueous AIB electrodes, focusing on the mechanisms of electrochemical activation, insertion, and conversion. However, no review has reported the fabrication of sustainable, low-cost, and high-power-density AIBs focusing on anode design, electrolyte selection, and cathode selection and preparation.

Herein, we summarize the current progress of AIBs and the corresponding opportunities, challenges and potential research directions (Fig. 1). We introduce the principles of AIBs, including the property of aluminum, electrochemical reactions, and components. Based on their electrochemical reactions and components, the challenges and outlooks of AIBs are reviewed from various perspectives, including anode design and protection, electrolyte exploitation and modification, and selection and preparation of cathode materials. We comprehensively discuss the acquisition of green and low-cost cathode materials with high-performance based on the requirements of AIBs and existing electrode materials.

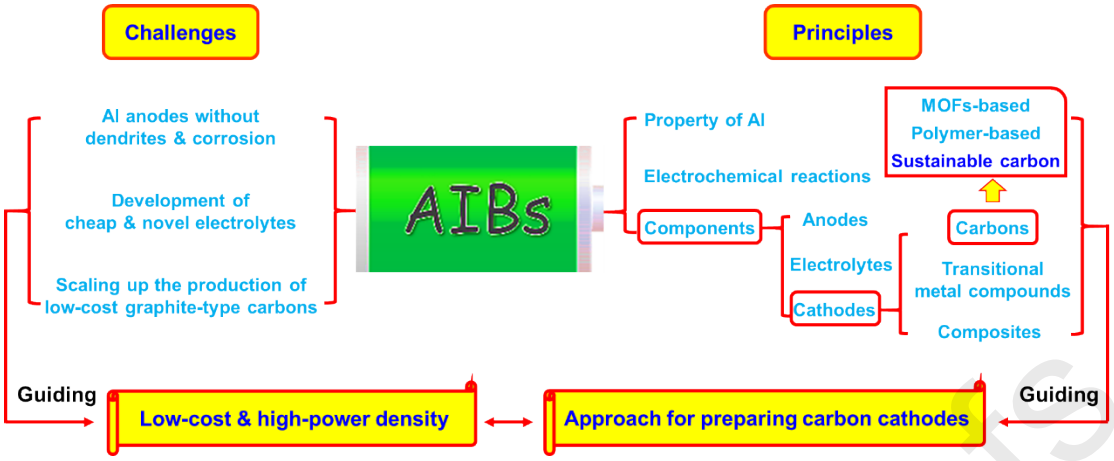

Fig. 1 Review scheme of opportunities, challenges, and potential research directions for AIBs.

2 Principles of AIBs

2.1 Property of aluminum

Al is a metal with an atomic number of 13. Table 1 lists the properties and electrochemical performance of this element. Table 1 also presents the characteristics of Li and Na in comparison with Al. In the Earth's crust, Li sources are limited and unevenly geometrically distributed [21]. Meanwhile, Al is the third most abundant element and the first most abundant metal [22]. Compared with Li, Al is extremely inexpensive because it can be produced through the electrolysis of aluminum oxide. Li, Na and Al have standard reduction potentials (E_0) of -3.045, -0.271 and -1.76 V, respectively. The drawback of Al is its higher atomic weight (26.98 a.m.u.) compared with Li (6.941 a.m.u.) [23]. Based on the equation (1), Al anode decreases the theoretical specific capacity of the battery system, but the three-electron redox reaction can increase its specific capacity compared with the one-electron redox reaction of Na. The theoretical specific capacity of 2980 mAh g^{-1} of Al is higher than that of sodium-

ion battery systems (Fig. 2a). Similar to lithium and sodium anodes [24, 25], aluminum anodes also face the challenge of dendrite formation due to the orientation of aluminum deposition during the electrochemical processes [26]. Moreover, Al can be oxidized in the air to form a surface passivation film of Al_2O_3, which prevents further reaction and stably exists in the air; it is easier to improve battery safety and stability. Thus, Al is more suitable than Li and Na for use in rechargeable batteries in terms of security and stability.

$$C_0=1000nF/3600M \quad (1)$$

where C_0 is the theoretical specific capacity, n is the number of electrons per molecule during redox reaction, F is the Faraday constant (96500 C mol^{-1}) and M is the Molar mass.

Table 1 Properties and electrochemical performance of Li, Na and Al.

Element	Li	Na	Al
Atomic number	3	11	13
Atomic mass (amu)	6.94	22.99	26.98
Density (g cm^{-3})	0.534	0.968	2.702
Melting point (°C)	180.54	97.72	660.37
Boiling point (°C)	1317	883	2467
Reserves	inhomogeneous and insufficient	6th in the earth's crust	3rd in the earth's crust
Standard reduction potential (V)	−3.045	−0.271	−1.676
Specific capacity (mAh g^{-1})	3870	1166	2980
Dendrite formation	Yes	Yes	Yes
React with oxygen	Yes	Yes	Yes
Stability in the air	No	No	Yes

2.2. Electrochemical reactions in AIBs

The electrochemical reaction of Al anode corresponds to the equation (2):

Anode:

$$Al+7AlCl_4^-\rightarrow 4Al_2Cl_7^-+3e^- \quad (2)$$

For the cathode, the electrochemical reactions correspond to Equations (3–14):

Carbon:

$$C_n+AlCl_4^-\rightarrow C_n[AlCl_4^-]+e^- \quad (3)$$

Metal oxide/sulfide:

$$WO_{3-x}+AlCl_4^-\rightarrow [AlCl_4]WO_{3-x}+e^- \quad (4)[27]$$

$$6CuO+2Al^{3+}+6e^-\rightarrow 3Cu_2O+Al_2O_3 \quad (5)[28]$$

$$AlV_3O_9+xAl^{3+}+3xe^-\rightarrow Al_{3+x-y}V_3O_{9-3y/2}+y/2Al_2O_3 \quad (6)[29]$$

$$MoS_2+xAl^{3+}+3xe^-\rightarrow AlxMoS_2 \quad (7)[30]$$

$$Co_3S_4+xAl^{3+}+3xe^-\rightarrow AlxCo_3S_4 \quad (8)[31]$$

$$SnS+nAlCl_4^-\rightarrow ne^-+SnS[AlCl_4^-]_n \quad (9)[32]$$

Composite, with high conductivity and good stability:

$$CoSe+4Al_2Cl_7^-+3e^-\rightarrow AlCoSe+7AlCl_4^- \quad (10)[33]$$

$$CoSe_2+mAl^{3+}+3me^-\rightarrow Al_mCo_nSe_2+(1-n)/Co \quad (11)[34]$$

$$Ni_{11}HP+mAl^{3+}+3me^-\rightarrow Al_mNi_nHP+(11-n)Ni \quad (12)[35]$$

$$Ni_2P+mAl^{3+}+3me^-\rightarrow Al_mNi_nP+(2-n)Ni \quad (13)[11]$$

$$SnO_2+4nAl_2Cl_7^-+3ne^-\rightarrow Al_nSnO_2+7nAlCl_4^- \quad (14)[36]$$

Lin et al. [8] constructed AIB in pouch cells (Fig. 2b) using an Al foil anode, a graphitic cathode, and an ionic liquid electrolyte made from vacuum-dried $AlCl_3$/1-ethyl-3-methylimidazolium chloride (EMIC). This cell exhibited distinct discharge

voltage plateaus in the ranges of 2.25–2.0 and 1.9–1.5 V, which delivered a discharge specific capacity of more than 60 mAh g^{-1} at a current density of 66 mA g^{-1} (1 C charging rate) (Fig. 2c). Cai et al. [34] designed an AIB by utilizing an Al foil anode, $AlCl_3$/EMIC electrolyte, and a $CoSe_2$/carbon nanodice@reduced graphene oxide (rGO) cathode. The cyclic voltammetry (CV) curve of the cell (Fig. 2d) showed two reduction peaks at ca. 0.9 and 1.8 V, while the corresponding oxidation peaks were observed at ca. 1.0 and 2.1 V, depending on the cathode material of $CoSe_2$/carbon nanodice@rGO.

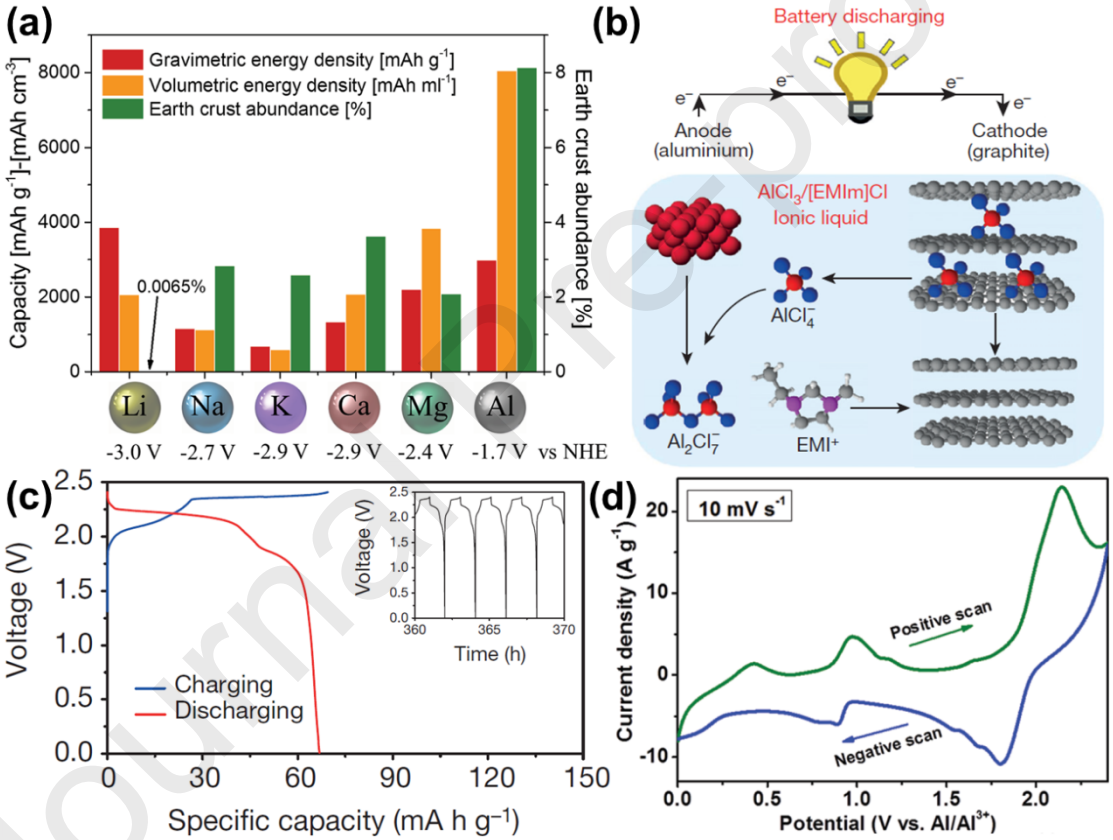

Fig. 2 (a) Comparison between gravimetric and volumetric capacities, standard reduction potential and heart crust abundance of metal anodes used or proposed for application in electrochemical storage systems [37]. Copyright 2016, Wiley. (b) Schematic of Al/graphite cell during discharge, with the optimal composition of the $AlCl_3$/[EMIm]Cl ionic liquid electrolyte. On the anode side, metallic Al and $AlCl_4^-$

were transformed into $Al_2Cl_7^-$ during discharge, and the reverse reaction occurred during charging. On the cathode side, $AlCl_4^-$ was predominantly intercalated and deintercalated between graphite layers during charge and discharge reactions, respectively. (c) Galvanostatic charge and discharge curves of an Al/pyrolytic graphite Swagelok cell at 66 mA g^{-1}. Inset: charge and discharge cycles [8]. Copyright 2015, Nature. (d) Typical CV curves at a scan rate of 10 mV s^{-1} [34]. Copyright 2018, Royal Society of Chemistry.

2.3 Components of AIBs

Table 2 Anodes, electrolytes, cathodes, and electrochemical performance of AIBs

Classification	Cathode	Electrolyte	Anode	Electrochemical performance			Ref.
				The highest capacity	At highest current density	Cycle life	
Graphite	Graphite	4.0 M $LiPF_6$ in ethyl methyl carbonate with vinylene carbonate additive	Al foil	104 mAh g^{-1} at 2 C	79 mAh g^{-1} at 5 C	A capacity retention of 88% after 200 cycles at 2 C	[3]
	Graphite	4.0 M $LiPF_6$ in ethyl methyl carbonate with vinylene carbonate additive	Porous Al	104 mAh g^{-1} at 2 C	85 mAh g^{-1} at 20 C	93 mAh g^{-1} at 2 C after 1000 cycles with 89.4% retention	[38]
	Graphite	4.0 M $LiPF_6$ in ethyl methyl carbonate with vinylene carbonate additive	Al nanosphere	105 mAh g^{-1} at 2 C	87 mAh g^{-1} at 20 C	88 mAh g^{-1} at 15 C after 1000 cycles with 94.6% capacity retention	[39]
	Graphite	$AlCl_3$ in 1-methyl-1-propylpyrrolidinium chloride	Al foil	75 mAh g^{-1} at 0.1 A g^{-1}	35 mAh g^{-1} at 0.1 A g^{-1}	-	[40]
	Graphite	$AlCl_3$ in Imidazole hydrochloride (ImidazoleHCl)	Al foil	129 mAh g^{-1} at 0.5 A g^{-1}	105 mAh g^{-1} at 4.0 A g^{-1}	A Coulombic efficiency of 99 % at 4.0 A g^{-1} after 1000 cycles	[41]
	Graphite	0.5 mol L^{-1} $AlCl_3$ in aqueous	Poly(3,4,9,10-perylentetracarboxylic diimide)	220 mAh g^{-1} at 0.05 A g^{-1}	95 mAh g^{-1} at 1.0 A g^{-1}	A capacity retention closed to 100% for 1000 cycles	[42]
	Graphite	$AlCl_3$/urea/CPL	Al foil	151 mA h g^{-1} at 5.0 A g^{-1}	105 mA h g^{-1} at 15 A g^{-1}	132 mA h g^{-1} with a Coulombic efficiency of 98% after 3000 cycles.	[43]
	Spherical graphite	$AlCl_3$ in pyridinium chloride	Al foil	123 mA h g^{-1} at 1.0 A g^{-1}	101 mA h g^{-1} at 5.0 A g^{-1}	a Coulombic efficiency of 97% after 500 cycles	[44]
	Prelithiation graphite	$AlCl_3$ in EMIC	Al foil	102.6 mAh g^{-1} at 0.1 A g^{-1}	49 mAh g^{-1} at 0.5 A g^{-1}	64 mAh g^{-1} at 0.2 A g^{-1} after 500 cycles with 95.1% retention	[45]
Graphene	Edge-rich graphene paper	$AlCl_3$ in EMIC	Al foil	128 mAh g^{-1} at 2 A g^{-1}	84 mAh g^{-1} at 10 A g^{-1}	90±3 mAh g^{-1} at 8 A g^{-1} after 20000 cycles	[46]
	Graphene nanoplatelets	$AlCl_3$ in trimethylamine hydrochloride	Al foil	134 mAh g^{-1} at 2 A g^{-1}	83 mAh g^{-1} at 4 A g^{-1}	A Coulombic efficiency above 98% over 3000 cycles	[47]
	Graphene aerogel	$AlCl_3$ in triethylamine hydrochloride	Al foil	112 mAh g^{-1} at 5 A g^{-1}	60 mAh g^{-1} at 25 A g^{-1}	112 mAh g^{-1} at 5 A g^{-1} after 30,000 cycles with 97.3% retention	[48]

	Graphene aerogel	$AlCl_3$ in EMIC	Al foil	245 mAh g^{-1} at 1 A g^{-1}	70 mAh g^{-1} at 15 A g^{-1}	without obvious capacity decay at 15 A g^{-1} after 5000 cycles	[49]
Polymer	Polypyrenes	$AlCl_3$ in EMIC	Al foil	100 mAh g^{-1} at 0.2 A g^{-1}	48 mAh g^{-1} at 2 A g^{-1}	100 mAh g^{-1} at 0.2 A g^{-1} after 1000 cycles	[50]
Metal oxide	WO_3 nanorods	$AlCl_3$ in EMIC	Al foil	118.9 mAh g^{-1} at 0.1 A g^{-1}	-	64.7 mAh g^{-1} at 0.1 A g^{-1} after 100 cycles	[27]
	Porous microspheric CuO	$AlCl_3$ in EMIC	Al foil	250.12 mAh g^{-1} at 0.05 A g^{-1}	112 mAh g^{-1} at 0.2 A g^{-1}	130.49 mAh g^{-1} at 0.05 A g^{-1} after 100 cycles	[28]
	$FeVO_4$	Aqueous $AlCl_3$ solution (ammonium hydroxide solution).	Al foil	350 mAh g^{-1} at 0.06 A g^{-1}	-	-	[12]
	3D hierarchical microsphere AlV_3O_9	$AlCl_3$ in EMIC	Al foil	327 mAh g^{-1} at 0.1 A g^{-1}	65.3 mAh g^{-1} at 0.4 A g^{-1}	195.5 mAh g^{-1} 0.1 A g^{-1} after 100 cycles	[29]
Metal sulfide	Porous Co_3S_4 microspheres	$AlCl_3$ in EMIC	Al foil	253.6 mAh g^{-1} at 0.02 A g^{-1}	77.7 mA h g^{-1} at 0.04 A g^{-1}	66.7 mA h g^{-1} at 0.04 A g^{-1} after 100 cycles	[30]
	SnS porous film	$AlCl_3$ in EMIC	Al foil	287.9 mAh g^{-1} at 0.05 A g^{-1}	80 mAh g^{-1} at 0.25 A g^{-1}	90 mA h g^{-1} at 0.05 A g^{-1} after 150 cycles	[31]
	VS_4/rGO	$AlCl_3$ in EMIC	Al foil	406 mAh g^{-1} at 0.02 A g^{-1}	106.5 mAh g^{-1} at 0.5 A g^{-1}	227 mA h g^{-1} at 0.1 A g^{-1} after 1000 cycles	[32]
Composite	Carbon-encapsulated CoSe nanoparticles	$AlCl_3$ in EMIC	Al foil	406.94 mAh g^{-1} at 0.1 A g^{-1}	60 mAh g^{-1} at 0.3 A g^{-1}	60 mAh g^{-1} at 0.3 A g^{-1} after 100 cycles	[51]
	Graphene-TiO_2 nanocomposite	$AlCl_3$ aqueous electrolyte	Al foil	427 mAh g^{-1} at 1 A g^{-1}	254.8 mAh g^{-1} at 5 A g^{-1}	62.4 mAh g^{-1} at 5 A g^{-1} after 100 cycles	[33]
	$CoSe_2$/carbon nanodice@rGO	$AlCl_3$ in EMIC	Al foil	52 mAh g^{-1} at 6.25 A g^{-1}	-	-	[52]
	$Ni_{11}(HPO_3)_8(OH)_6$/rGO nanorods	$AlCl_3$ in EMIC	Al foil	326 mAh g^{-1} at 1 A g^{-1}	-	143 mAh g^{-1} at 1 A g^{-1} after 500 cycles	[34]
	Ni_2P/rGO nanosheets	$AlCl_3$ in EMIC	Al foil	182.0 mAh g^{-1} at 0.2 A g^{-1}	-	49.2 mAh g^{-1} at 0.2 A g^{-1} after 1500 cycles	[35]
	SnO_2/C Nanocomposite	$AlCl_3$ in EMIC	Al foil	274.5 mAh g^{-1} at 0.1 A g^{-1}	60.9 mAh g^{-1} at 0.2 A g^{-1}	60 mAh g^{-1} after 3000 cycles at 0.2 A g^{-1}	[11]
	Co_9S_8@ carbon nanotubes	$AlCl_3$ in EMIC	Al foil	434 mAh g^{-1} at 0.05 A g^{-1}.	-	72 mAh g^{-1} at 2 A g^{-1} after 20000 cycles	[36]
				315 mAh g^{-1} at 0.1 A g^{-1}	154 mAh g^{-1} at 1 A g^{-1}	87 mAh g^{-1} at 1 A g^{-1} after 6000 cycles	[9]

2.3.1 Anode

Al has long attracted attention as a potential battery anode because of its high theoretical voltage and specific energy [53-55]. Al can be electrodeposited and is therefore suitable for the development of rechargeable batteries. Considerable efforts have been exerted to develop rechargeable AIBs with high power density [56]. Similar to other battery systems, the dissolution/deposition kinetics of metal anodes play crucial roles in the charge and discharge speed, directly affecting the power density of AIBs [57]. Moreover, the dendrite growth is also a major challenge during electrochemical processes [58, 59]. Long et al. [60] tracked the dendrite growth process and recorded the Al deposition by in-situ optical microscopy at a current density of 10 mA (Fig. 3a). Fluffy Al started to form, protrusions of dendritic Al became visible, more dendrites shoot out in an obvious tip-growth manner, the “dead” Al dendrites fell off. It demonstrated the dendrite issue in Al metal batteries. Increasing the specific surface area of metal anodes, such as porous electrodes and powder electrodes, can effectively regulate the dissolution/deposition kinetics and the charge distributions [61-63], guiding the design of high-power-density AIBs without anode dendrite formations.

Based on the above principles, Tong et al. [38] designed a porous Al foil anode for high-rate AIBs. The porous Al foil coated with a uniform carbon layer (pAl/C) was fabricated by etching, deposition, solidification of polyacrylonitrile, and subsequent carbonization (Fig. 3b). The 3D porous Al structure provides fast ion/electron transport channels and sufficient space to accommodate volume expansion during electrochemical processes. The AIB cell with the pAl/C anode and natural graphite

cathode exhibited reversible capacities of 104 and 85 mAh g^{-1} at 2 and 20 C, respectively (Figs. 3c and 3d). Moreover, the cell demonstrated a retention capacity of 93 mAh g^{-1} at 2 C after 1000 cycles without dendrite growth, with 89.4% retention and a power density of 3084 W kg^{-1}. To further increase the electrochemical reaction rate, Tong et al. [39] developed dendrite-free core/shell Al@carbon nanospheres (nAl@C) anode composed of Al nanospheres and an amorphous carbon outer layer (Fig. 3e). The cell with nAl@C anode and graphite cathode exhibited a capacity of 88 mA h g^{-1} with a capacity retention of 94.6%, a Coulombic efficiency of 99.5% after 1000 cycles at 15 C (Fig. 3f), and a power density of 3701 W kg^{-1}. Compared with the Al foil [3], the discharge speed and power density were significantly improved owing to the enhancement of specific surface area. In addition to enhancing power density, porous and powder anodes with micron or sub-micron sizes are effective ways to suppress dendrite formation during dissolution/deposition [38, 39]. Therefore, the specific surface area improvement of Al anode through structure design can be the key to increase the power density of AIBs, which will be the focus of future research.

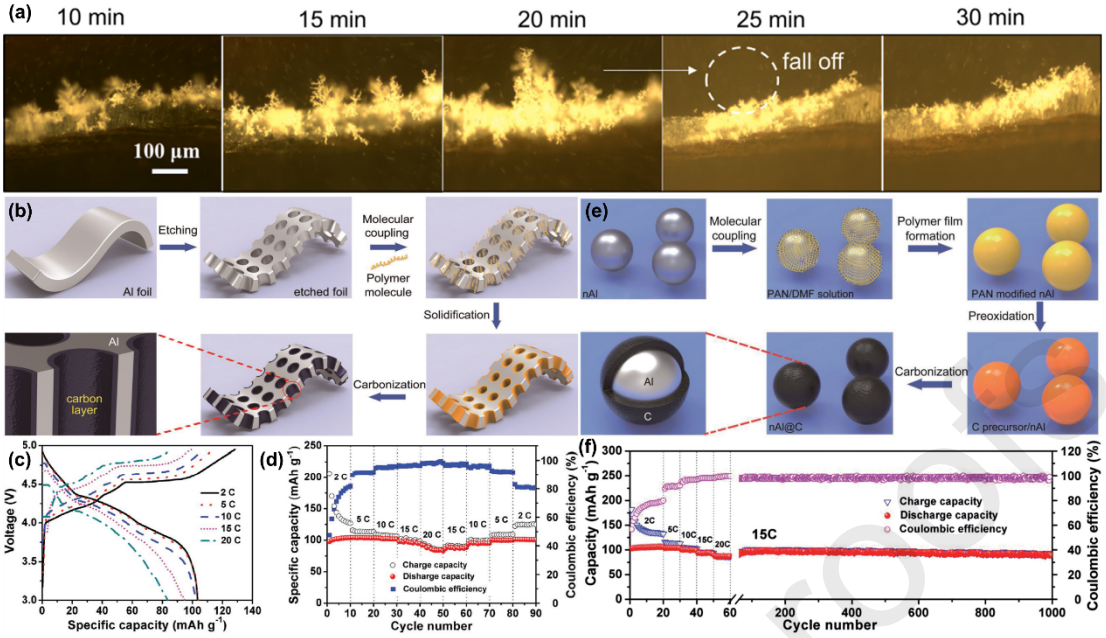

Fig. 3 (a) In-situ optical microscopic observation of Al dendrite formation on planar Al [60]. Copyright 2021, Elsevier. (b) Schematic of the fabrication process of pAl/C anode material. (c) Charge–discharge curves of the pAl/C-graphite battery at different current rates from 2 C to 20 C at the sixth cycle for each current rate. (d) Corresponding capacities and Coulombic efficiencies at different current rates [38]. Copyright 2016, Wiley. (e) Schematic of nAl@C fabrication process. (f) Charge–discharge curves at different current rates and the long-term cycling stability at 15 C for 1000 charge–discharge cycles of the nAl@C–graphite battery [39]. Copyright 2018, Wiley.

2.3.2 Electrolyte

The electrolyte plays a vital role in the battery systems, ensuring fast ion transport in the internal circuit [24, 64]. The [EMIm]AlxCly electrolyte with an ion conductivity of 9.41 mS cm^{-1} at room temperature sufficiently meets the requirement of high-power AIBs [48]. However, this kind of electrolyte severely restricts the grid-scale application

and industrialization of AIBs due to the high cost of EMIC. Developing cheaper electrolytes is highly desired for the fabrication of low-cost and high-power AIBs [65]. A low-cost $AlCl_3$/NaCl molten salt was developed for an AIB with performances of 190 and 60 mAh g^{-1} at 0.1 and 4 A g^{-1} [66], respectively, but an external heat of 120 °C was required to maintain the salt-based electrolyte. The development of a low-cost and room-temperature electrolyte enabling AIBs with high power density remains a great challenge.

In general, $AlCl_3$ is selected as the metal salt. Thus, the choice and optimization of solvents, such as 1-methyl-1-propylpyrrolidinium chloride (Py13Cl), EMIC, and Et_3NHCl, is important in the exploration of electrolytes. In this respect, Zhu et al. [40] designed an ionic liquid for AIBs by mixing Py13Cl with $AlCl_3$ (Fig. 4a). The Py13Cl–$AlCl_3$ ionic liquid exhibited lower density (Fig. 4b), higher viscosity (Fig. 4c), and lower conductivity (Fig. 4d) than its EMIC-$AlCl_3$ counterpart. To improve the electrochemical performance, Xu et al. [48] fabricated an $AlCl_3$/Et_3NHCl ionic liquid electrolyte for high-power AIB systems. The higher bonding energy of $AlCl_3$/Et_3NHCl led to a higher viscosity than the EMIC-based cases, exhibiting better stability, higher decomposition voltage, and wider potential window than the $AlCl_3$/Et_3NHCl system (Figs. 4e and 4f). The cell showed a 112 mAh g^{-1} capacity with 97.3% retention after 30,000 cycles (Fig. 4g) and 84% retention at a current density of 18 A g^{-1} (150 C and 18 s charging; Fig. 4h).

Based on the recent research progress, the development of highly efficient AIB electrolyte should focus on the exploration of suitable solvents [16], such as organic

polyester {1-trifluoroacetyl piperidine-based electrolyte (TFAP), pyridinium chloride, Imidazole hydrochloride, trimethylamine hydrochloride (TMAHCl), 1-ethyl-3-methylimidazolium chloride [67], and urea [68] ect.} and an aqueous solution (i.e. water). Elterman et al. [69] developed a novel TFAP-based electrolyte for AIBs, the specific conductivities at 30 ^{o}C of series $AlCl_3$/TFAP, $AlCl_3$/LiCl/TFAP, TFAP/[EMIm]Cl/$AlCl_3$ were 0.49, 0.28 and 1.37 mS cm^{-1}, respectively. The exchange current densities at the two-phase interface aluminium/electrolyte were 0.18, 0.03 and 0.42 mA cm^{-2}, respectively. TFAP-based electrolytes did not crystallize when cooled down to 60 ^{o}C. Xu et al. [44] reported an $AlCl_3$/pyridinium chloride electrolyte for AIB with Al anode and spherical graphite cathode, showing a discharge capacity of 123 mA h g^{-1} at 1.0 A g^{-1}, and a discharge capacity of 101 mA h g^{-1} at 5 A g^{-1} with a Coulombic efficiency of 97% after 500 cycles. Xu et al.[41] prepared an AIB with $AlCl_3$/Imidazole hydrochloride electrolyte, aluminum anode and graphite cathode, achieving a specific discharge capacity of 129 mAh g^{-1} at 0.5 A g^{-1} and 105 mA h g^{-1} with a Coulombic efficiency of 99 % at 4 A g^{-1} after 1000 cycles. Cang et al. [42] reported poly (3,4,9,10-perylentetracarboxylic diimide) anode for aqueous AIB with 0.5 mol L^{-1} $AlCl_3$ electrolyte, delivering a specific capacity close to 99% capacity retention after 1000 cycle and a reversible capacity of 185 mAh g^{-1} at 0.1 A g^{-1} with a Coulombic efficiency close to 100%. Ng et al. [47] reported a AIB with Al anode, $AlCl_3$/TMAHCl (Fig. 4i) ionic liquid electrolyte and graphene nanoplatelets cathode, delivering a specific capacity of 134 mAh g^{-1} at 2.0 A g^{-1} with a Coulombic efficiency above 98% for 3000 cycles (Fig. 4j). $AlCl_3$/TMAHCl electrolyte opens up a new avenue for the development

of AIBs due to the low-cost and high performance.

In addition, Xu et al. [43] prepared $AlCl_3$/caprolactam (CPL) and $AlCl_3$/urea/CPL for AIBs. The $AlCl_3$/CPL electrolyte exhibited a specific capacity of 136 mA h g^{-1} at 5.0 A g^{-1}. The $AlCl_3$/urea/CPL electrolyte achieved a high initial specific capacity of 151 mA h g^{-1} at 5.0 A g^{-1} and reached 132 mA h g^{-1} with a high Coulombic efficiency of 98% after 3000 cycles. Please see Fig. 4k, $AlCl_3$/CPL as the electrolyte, $AlCl_4^-$ intercalated into C layers and formed $CxAlCl_4$ on the cathode during charging; $Al_2Cl_7^-$ decomposed into Al and $AlCl_4^-$ on the anode. When urea was added to the $AlCl_3$/CPL electrolyte, $[AlCl_2 \cdot (urea)_2]^+$ would break down into Al, $AlCl_4^-$, and urea. Park et al. [70] proved that benzene was a good electrolyte organic additive, the diffusion coefficients were increased from 2.348×10^{-8} to 14.634×10^{-8} cm^2 S^{-1} for the electrolytes containing 45% benzene. It provides a guiding direction for the development of high-performance electrolyte by addition of organic additive.

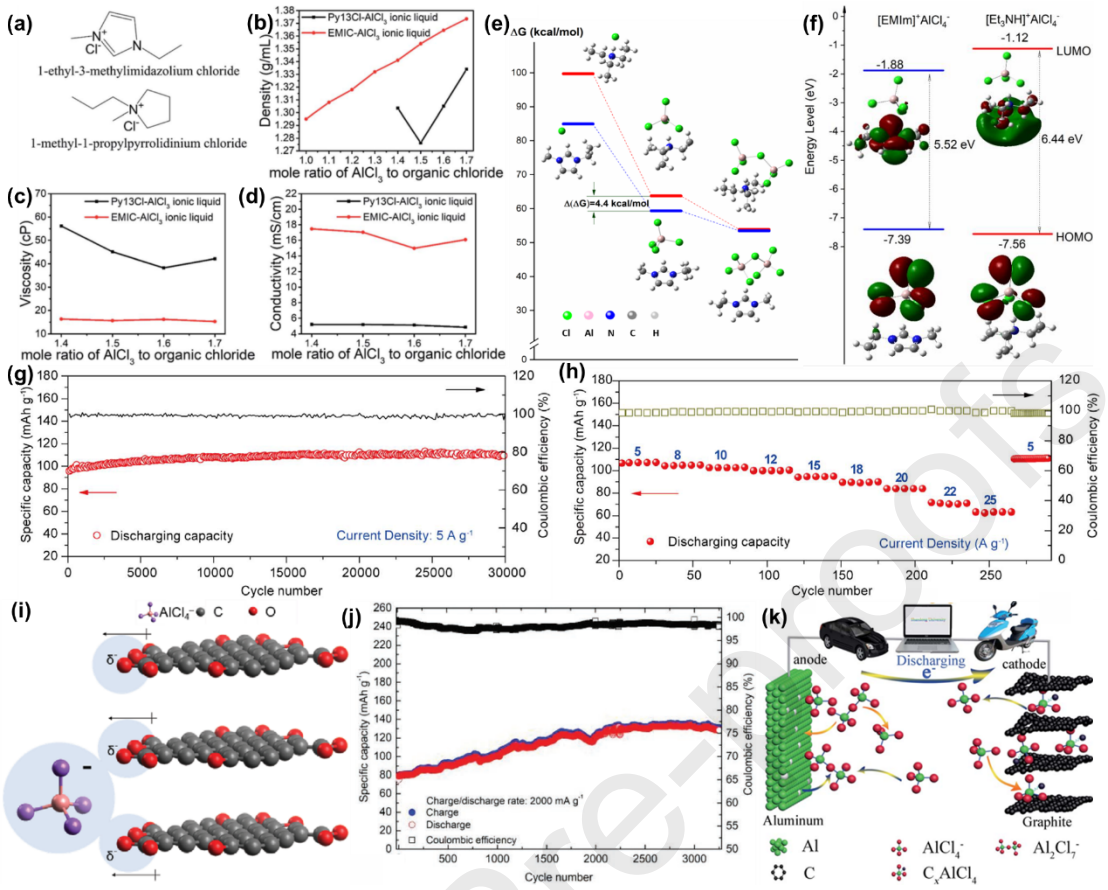

Fig. 4 (a) Structure of EMIC and Py13Cl, (b) density comparison between Py13Cl–$AlCl_3$ and EMIC-$AlCl_3$, (c) viscosity comparison between Py13Cl–$AlCl_3$ and EMIC-$AlCl_3$ measured at 23 °C–24 °C. (d) Conductivity comparison between Py13Cl–$AlCl_3$ and EMIC-$AlCl_3$ measured at 25 °C [40]. Copyright 2019, Royal Society of Chemistry. (e) Density functional theory (DFT) calculated bonding energies of Et_3NH^+ and $[EMIm]^+$ with Cl^-, $AlCl_4^-$, and $Al_2Cl_7^-$ with ΔG (kcal/mol) energies using B3LYP/6–311++G(d,p) method. (f) Highest-occupied molecular orbital and lowest-occupied molecular orbital plots of $[EMIm]^+AlCl_4^-$ and $[Et_3NH]^+AlCl_4^-$ calculated by DFT. (g) Galvanostatic cycling over 3,000 cycles (current density at 5 A g^{-1} and 2.54 V/0.7 V upper/lower cut-off voltage). (h) Rate capability at different charge/discharge current densities from 5 A g^{-1} to 25 A g^{-1} [48]. Copyright 2019, Elsevier. (i) A schematic

diagram illustrating the repulsion between $AlCl_4^-$ and functional groups near the edges of graphene planes during intercalation. (j) Galvanostatic cycling over 3000 cycles [47]. Copyright 2020, Wiley. (k) Schematic drawing of AIBs using $AlCl_3$/CPL or $AlCl_3$/urea/CPL as the electrolytes [43]. Copyright 2020, Royal Society of Chemistry.

2.3.3 Cathode

In AIBs, the introduction of various high-performance cathodes is an effective strategy for improving their reversibility and electrochemical performance. We summarize recent research progress on cathode materials and compare them in Table 2 and Fig. 5.

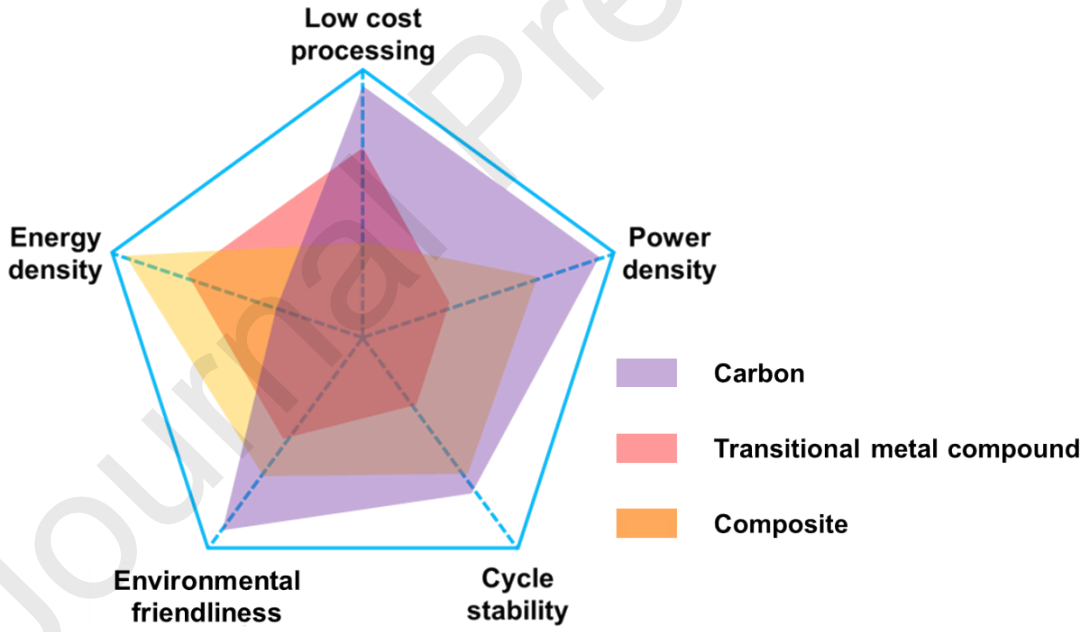

Fig. 5 Feature comparison of carbon, transitional metal compound, and composite cathodes.

2.3.3.1 Carbon

Carbonaceous materials are promising cathode materials for AIBs. Graphite is an attractive cathode material for energy storage because it allows reversible intercalation/deintercalation of numerous compound anions at high potentials [71, 72]. Natural graphite has been investigated as a cathode for AIBs. However, several drawbacks of natural graphite, such as severe volume swelling, shorten its lifetime [73]. Wei et al. [73] prepared a composite material by depositing amorphous carbon on graphite paper, which exhibited a longer cycle life than normal graphite paper. The interface between the amorphous carbon and graphite paper allowed $AlCl_4^-$ to diffuse faster by overcoming less energy barrier than the two graphene layers. Zhang et al. [74] demonstrated that graphite with a high crystallinity and nanosheet-bricked porous structure can be a good cathode for AIBs. The high crystallinity and thin layer characters facilitate the high-capacity and high-rate storage of Al^{3+}. Therefore, interface control and microstructure design of carbon cathode materials can be the key to manufacturing high-power-density AIBs.

Zhang et al. [45] synthesized the prelithiation graphite cathode material for AIBs by treatment with n-butyllithium (Fig. 6a). Not only $AlCl_4^-$ but also Al^{3+} can be intercalated and deintercalated into the prelithiation graphite cathode because the interlayer spacing was improved by prelithiation treatment, which reduced the electrostatic effect between $AlCl_4^-$ or Al^{3+} and the cathode materials. In addition to the graphite system, other carbon materials, such as polymers, can be used as AIB cathode. Walter et al. [50] prepared a cathode based on inexpensive pyrene polymers with a capacity of 100 mAh g^{-1} at a discharge voltage of 1.7 V, energy efficiency of 86%, and

cyclic stability of 1000 cycles (Fig. 6b). During charging (Fig. 6c), the condensed aromatic rings of these polymers were oxidized, accompanied by the uptake of $AlCl_4^-$ from the chloroaluminate ionic liquid. Discharge involved the fast inverse process of reduction and the release of $AlCl_4^-$. For the microstructure design, Huang et al. [49] reported the facile construction of nanoporous densely stacked films derived from 3D graphene aerogels (GAs), prepared by self-propagating combustion reduction of GO aerogels, as an advanced binder-free cathode for high-power-density and high-capacity AIBs (Fig. 6d). Owing to the characteristics of 3D interconnected nanoporous structure, a large surface area (513 $m^2\ g^{-1}$), high electrical conductivity (581 S cm^{-1}), dense stacking (0.61 g cm^{-3}), and expanded interlayer spacing (3.69 Å) of GA-derived compact film, the AIB cell delivers a high capacity of 245 mAh g^{-1} at 1 A g^{-1}, which is at least twice that of graphite for AIBs. To reduce the cost, Zhang et al. [46] presented the low-temperature (600 °C) synthesis of edge-rich graphene paper (Fig. 6e) for the cathode of AIBs with a capacity of 128 mA h g^{-1} at 2 A g^{-1} (Fig. 6f) and a Coulombic efficiency higher than 99.2% after 20,000 cycles at 8 A g^{-1} (Fig. 6g).

Despite the increased power density and discharge capacity of carbonaceous cathodes in AIBs, more research are needed to carry out investigations on the specific surface area improvement, porosity enhancement, and carbon layer spacing adjustment to enhance the capacity of AIBs. Moreover, simple, inexpensive, and low-temperature synthesis methods can be the focus of carbon cathode development.

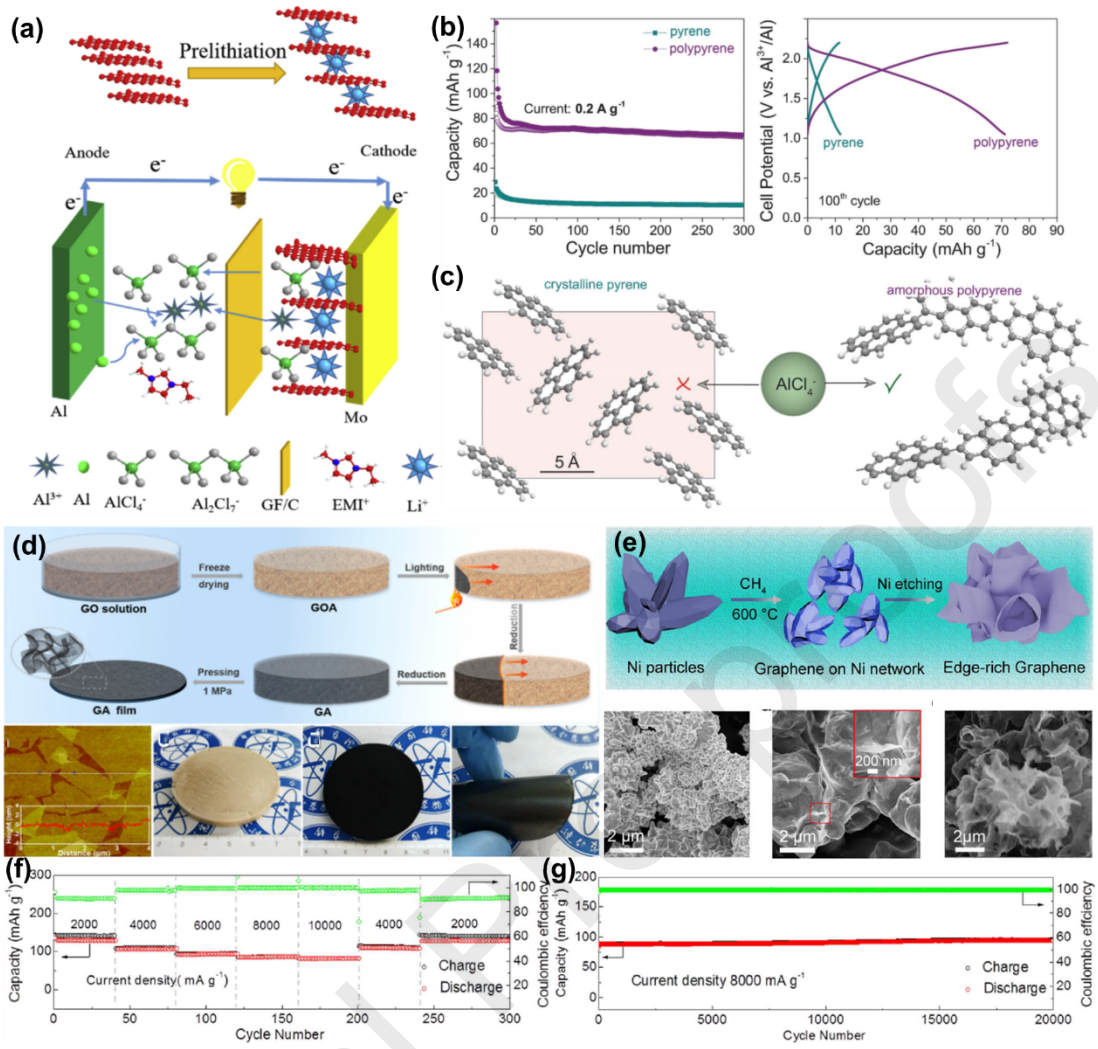

Fig. 6 (a) Schematics of graphite prelithiation treatment and AIB during the discharging process [45]. Copyright 2018, Elsevier. (b) Electrochemical performance of AIBs with pyrene and polypyrene cathodes. (c) Schematic of structural differences between pyrene and polypyrene that affect their $AlCl_4^-$ storage behavior [50]. Copyright 2018, Wiley. (d) Illustration of the fabrication process of GA film cathode [49]. Copyright 2019, Elsevier. (e) Schematic of the low-temperature synthesis of edge-rich graphene. Ni particles were used as 3D scaffold template for chemical vapor deposition (CVD) growth of graphene, followed by etching. Scanning electron microscopy (SEM) images of Ni particles, graphene on Ni network, and edge-rich graphene. (f) Rate performance

of edge-rich graphene cathode at 2, 4, 6, 8, and 10 A g^{-1}. (g) Galvanostatic cycling of edge-rich graphene (8 A g^{-1}) over 20,000 cycles [46]. Copyright 2018, Elsevier.

2.3.3.2 Transitional metal compounds

In addition to carbon materials, various transitional metal compounds, mainly including transitional metal oxides (V_2O_5 and TiO_2) and chalcogenides (Ni_3S_2, SnS_2, and Mo_6S_8), have been explored as cathodes for AIBs [75-79]. Layered transition metal oxides can be important cathode materials based on multivalent ions [80]. For example, in the layered-type molybdite (α-MoO_3) as a cathode for AIBs, aluminum cation is intercalated in the interlayer space between the octahedron layers (MoO_6), whereas the main framework is preserved [81]. Chemical defects also play an important role in AIB cathode design. Tu et al. [27] synthesized a series of WO_{3-x} nanorods with oxygen vacancies by hydrothermal process (Fig. 7a) and subsequent thermal reduction (Fig. 7b). The increase in surface oxygen vacancies is beneficial for the high discharge plateau and improvement of energy density. The pore structure in the metal oxide electrode is also significant, but lower conductivity leads to lower Coulombic efficiency. Zhang et al. [28] synthesized porous microspheric CuO (PM-CuO) composed of numerous stacked bitty nanorods for AIBs by using a one-pot hydrothermal process. The PM-CuO possessed a specific surface area of 21.61 m^2 g^{-1} and pore volume value of 0.179 cm^3 g^{-1} and exhibited a discharge capacity of 250.12 mA h g^{-1} at 0.05 A g^{-1}. However, good cycle performance also needs to be achieved through the improvement of structural stability. Li et al. [29] prepared a 3D hierarchical microsphere AlV_3O_9

electrode material composed of nanosheets (Fig. 7c) for AIBs. Al^{3+} reversibly intercalated and de-intercalated into the AlV_3O_9 electrode material, and phase transition occurred at the electrode material interface. The AlV_3O_9 cathode exhibited a discharge specific capacity of 317 m A h g^{-1} at 0.1 A g^{-1}, and the Coulombic efficiency was close to 100% (Fig. 7d). The capacity retention rate was only 61.7% after 100 cycles.

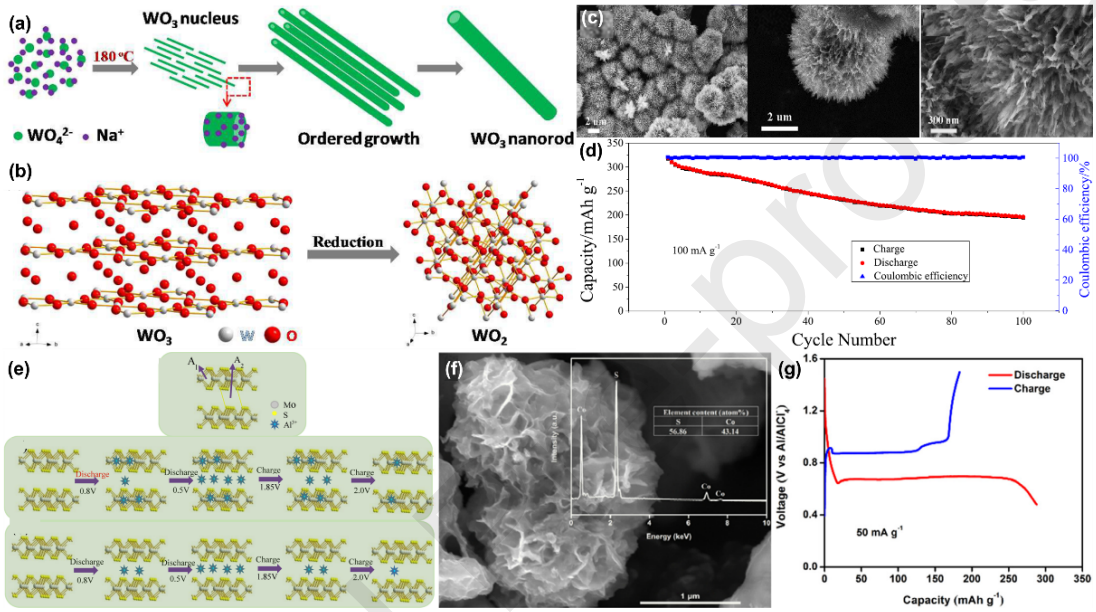

Fig. 7 (a) Schematic of the formation process of WO_3 nanorods. (b) Schematic of the introduction of oxygen vacancies during the thermal reduction process [27]. Copyright 2018, Royal Society of Chemistry. (c) SEM image of AlV_3O_9. (d) Cycle performance and Coulombic efficiency of AlV_3O_9 electrode material at 0.1 A g^{-1} [29]. Copyright 2019, Elsevier. (e) Crystal structure of MoS_2; Al^{3+} intercalated and deintercalated into MoS_2 microspheres at the electrode material interface and internal [30]. Copyright 2018, American Chemical Society. (f) SEM image and energy dispersive spectroscopy spectrum of Co_3S_4 microspheres. (g) Initial discharge/charge curves of Co_3S_4 cathode at 0.05 mA g^{-1} [31]. Copyright 2019, Elsevier.

Transitional metal chalcogenides show great advantage in electrochemical capacity compared with other materials due to their higher number of active sites for accommodating cations [48, 49]. Li et al. [30] fabricated a MoS_2 microsphere cathode for AIBs; the packing of MoS_2 units had two different positions for intercalated and deintercalated Al^{3+}, where the smaller site A1 was consisted of S−Mo−S ion bonds, and the larger site A2 was constructed by individual MoS_2 layers separated by van der Waals gap (Fig. 7e). The constructed cathode showed a discharge specific capacity of 253.6 mA h g^{-1} at 0.02 A g^{-1} and a discharge capacity of 66.7 mA h g^{-1} at 0.04 A g^{-1}, such high-rate performance needs to be improved urgently. Li et al. [31] demonstrated porous Co_3S_4 microsphere as an AIB cathode material (Fig. 7f). The cell underwent Al^{3+} intercalation/deintercalation with Co^{3+}/Co^{2+} as a redox couple in the cathode. The diffusion of Al^{3+} in the host Co_3S_4 is the key kinetic step that limited the discharge/charge current density. At 0.05 A g^{-1}, the Co_3S_4 cathode delivered a discharge capacity of 287.9 mA h g^{-1} with a long smooth voltage plateau of 0.68 V (Fig. 7g), the charge/discharge capacity was only ~90 mAh g^{-1} after 150 cycles. Liang et al. [32] fabricated a SnS porous film as a cathode material in AIB, the film delivered a specific capacity of 406 mAh g^{-1} at 0.02 A g^{-1}. The low conductivity and weak structural stability of transition metal compounds result in poor rate performance and low cycle performance; thus it requires further adjustments in the compositions and structures of the cathode materials for high performance AIBs.

2.3.3.3 Composite

Although carbon cathodes deliver lower specific capacities in comparison with metal compounds, their stable cycling capability allows them to offer more promising future for serviceable AIBs [45, 73]. Composite electrodes with metal oxides/sulfides and carbon are expected to exhibit improved electrochemical performance [48, 56, 57]. Composite cathodes combine a carbon material and a metal compound by a specific method and can simultaneously exert the advantages of both types of materials. Zhang et al. [51] prepared a VS_4/rGO composite cathode with flower-like microstructure, showing good conductivity, high specific surface area and being conducive for ion storage, thus inhibiting volume expansion during charging/discharging processes and improving the charge and discharge velocity. It delivered an initial charge/discharge specific capacities approaching 491.57 and 406.94 mAh g^{-1}, respectively, at 0.1 A g^{-1} between 0.1 and 2.0 V versus Al/$AlCl_4^-$. Xing et al. [33] developed a 3D carbon-encapsulated cobalt selenide nanoparticles from metal organic frameworks (MOFs) as AIB cathode. At 5 A g^{-1}, the initial discharge capacity of the cathode can reach 254.8 mAh g^{-1}, and a capacity of 62.4 mAh g^{-1} was retained after 100 cycles, attributing to the well-defined nanostructure of three-dimensional carbon-encapsulated cobalt selenide cathode material. Lahan et al. [52] addressed the phenomenon of Al^{3+} intercalation–deintercalation in TiO_2/graphene nanocomposite. Graphene formed an electronically conducting percolation network around TiO_2, serving as a driving force for facile Al^{3+} ion diffusion. The incorporation of graphene was assumed to enhance the Al^{3+} diffusion coefficient in TiO_2 by 44 times ($D_{TiO_2\ NP} \propto 0.082^2$ to $D_{G\text{-}TiO_2\ NP} \propto 0.5443^2$). The TiO_2/graphene nanocomposite delivered a discharge

capacity of 52 mAh g^{-1} at 6.25 A g^{-1}, and the reversible crystal phase transition was from TiO_2 to Al_2TiO_5 due to Al^{3+} intercalation–deintercalation.

Cai et al. [34] reported the $CoSe_2$/carbon nanodice@rGO cathode for AIBs. The results revealed that energy storage involved the incorporation of Al^{3+} into $CoSe_2$ to generate $Al_mCo_nSe_2$ and elemental Co (Fig. 8a), whereas capacity deterioration resulted from the dissolution of active cobalt species into the electrolyte and pulverization of the $CoSe_2$ phase (Fig. 8b). The $CoSe_2$/carbon nanodice@rGO cathode displayed a capacity of 143 mA h g^{-1} at 1 A g^{-1} after 500 cycles because of enhancing the structural stability and increasing composite conductivity. Tu et al. [35] investigated the electrochemical behaviors of the ultrashort $Ni_{11}(HPO_3)_8(OH)_6$ nanorods supported on rGO ($Ni_{11}(HPO_3)_8(OH)_6$/rGO nanorods) as a candidate for cathodic applications in AIBs. The results indicate that rGO is beneficial for the improvement of the energy density of $Ni_{11}(HPO_3)_8(OH)_6$ for AIBs (Fig. 8c). In AIBs (Fig. 8d), $Ni_{11}(HPO_3)_8(OH)_6$ is partially substituted with Al^{3+} to form $Al_mNi_n(HPO_3)_8(OH)_6$ and metallic Ni in the nanorod-like $Ni_{11}(HPO_3)_8(OH)_6$ cathodes during the discharge process. Tu et al. [11] reported a nickel phosphide nanosheet supported on rGO (Ni_2P/rGO nanosheets) for AIBs. The energy storage mechanism involves the incorporation of Al^{3+} into Ni_2P, generating Al_mNi_nP and elemental Ni (Fig. 8e). It is ascribed to the uniform morphology and incorporated structure with Ni_2P nanosheets supported on a reduced graphene oxide matrix, as well as the uniform reduced graphene oxide distribution; these can be propitious to the improved electronic conductivity and high active surface area. Ni_2P/rGO revealed a reversible capacity of 60 mAh g^{-1} over 3000 cycles at 0.2 A g^{-1}

(Fig. 8f). Lu et al. [36] reported a porous carbon-supported SnO_2 nanocomposite as a cathode material for AIB. The cell retained a stabilized discharge capacity of 72 mA h g^{-1} after 20,000 cycles with a Coulombic efficiency of ~100% at 2 A g^{-1} (Fig. 8g) because the conductive porous carbon framework facilitated an enhanced ion/electron diffusion pathway. Hu et al. [9] reported a binder-free and self-standing cobalt sulfide encapsulated in carbon nanotubes as a novel cathode material for AIBs. Abundant porous structure improves the electrolyte infiltration into the electrode and allows more active sites to be exposed, facilitating the kinetic processes; the binder-free and free-standing characteristics decrease the possibility of active material disintegration and side reaction, increasing the electrochemical stability. Therefore, the cathode material exhibited a cycling capacity of 87 mA h g^{-1} after 6000 cycles at 1 A g^{-1} (Fig. 8h). Despite these efforts, commercial AIBs are still limited by the lack of suitable cathode materials, which should possess high C rate capacity, good stability, low cost, and simple synthesis method, with high capacity and long cycle life [18, 37].

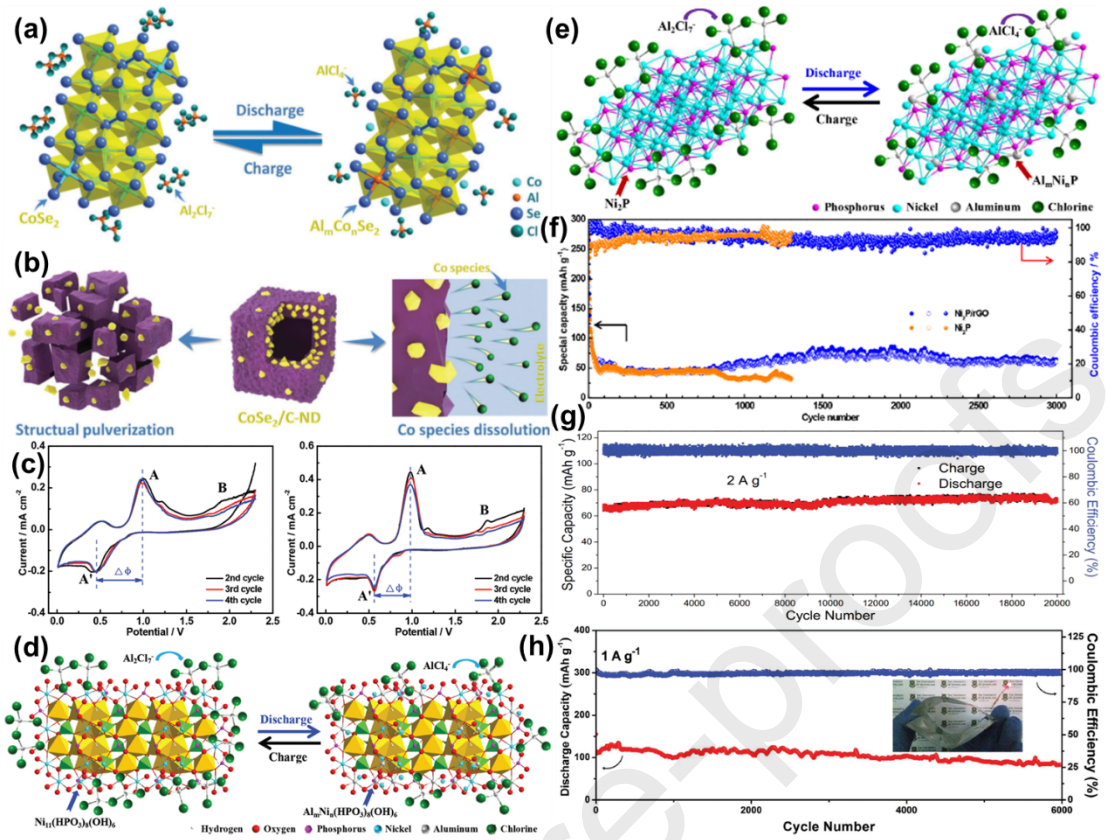

Fig. 8 Schematic of the proposed energy storage (a) and capacity-deterioration (b) mechanisms for the $CoSe_2$-based composite cathode [34]. Copyright 2018, Royal Society of Chemistry. (c) CV curves from the 2nd to 4th cycle of $Ni_{11}(HPO_3)_8(OH)_6$ and $Ni_{11}(HPO_3)_8(OH)_6$/rGO cathodes at a scan rate of 0.5 mV s^{-1} between 0.01 and 2.3 V vs. Al^{3+}/Al. (d) Schematic of the proposed redox reaction mechanism of the $Ni_{11}(HPO_3)_8(OH)_6$ cathode [35]. Copyright 2018, Royal Society of Chemistry. (e) Schematic of the energy storage mechanism of the Ni_2P cathode for AIBs. (f) Long-term cycling performance of Ni_2P and Ni_2P/rGO electrodes at a current density of 200 mA g^{-1} [11]. Copyright 2019, American Chemical Society. (g) Discharge/charge capacity and Coulombic efficiency of SnO_2/C cells within a voltage window of 0.05–1.95 V vs. Al/Al^{3+} at a current density of 2 A g^{-1} [36]. Copyright 2018, Royal Society of Chemistry. (h) Specific discharge capacity and Coulombic efficiency versus cycle

number with Co_9S_8@CNT–CNF electrode at a current density of 1 A g^{-1} [9]. Copyright 2018, Wiley.

3 Challenges

Several progresses have been made in the study of AIBs, which can withstand a charge–discharge current density of up to 25 A g^{-1} [48]. However, the large-scale practical application of AIBs with the features of green, low cost, and high power density still faces numerous challenges (Fig. 9).

First, as a simple anode material, metallic Al changes from Al foil to Al foam to Al powder, resulting in an ever-increasing current density of the battery due to the enhancement of specific surface area [38] [39]. The manufacturing technology of Al powder is very mature [82], but the preparation of large-scale AIB anode directly affects the battery performance. Fixing Al powder with other binders in electrodes can seriously affect the conductivity and uniformity of electrodes. Non-uniform structures may cause the growth of metal dendrites, resulting in battery decay or short circuit [26]. Thus, the rational design of the Al powder anode without dendrites and corrosion is still a major challenge that must be overcome to realize the practical application of high-performance AIBs.

Second, the electrolyte determines the ionic conductivity of the circuit inside batteries. However, the types of electrolytes for AIBs, such as EMIC and Py13Cl-based electrolytes, are currently limited [48]. Thus, the choice of electrolytes for AIB design are also limited. In addition, such electrolytes are expensive. The development of cheap

and novel electrolytes is another major challenge.

Third, the specific capacity of Al is 2980 mAh g^{-1}, whereas that of the cathode is below 500 mAh g^{-1} [51]. Similar to lithium ion batteries, the main reason for limiting the performance of AIBs is the cathode material [83]. Common cathode materials mainly include carbon materials, metal compounds, and composite materials. The selection and preparation of cathode materials are the primary challenges in the development of green, low-cost, and high-power-density AIBs. For the most potential carbon cathode, the electrochemical performance is profoundly dependent on the type and processing conditions [19]. The production of graphite-type carbon requires special techniques and an extremely high temperature (~3000 °C) [2]. Therefore, scaling up the production at reduced cost and obtaining graphite-type carbon are formidable tasks.

Fig. 9 The challenges of AIBs.

4 Approach for preparing carbon cathodes

Carbon is a promising electrode material for low-cost AIBs, because it not only

possesses good mechanical properties but also a high electronic conductivity [84-86]. Good mechanical properties can preserve the integrity of electrodes via accommodating the volume change during cycling, whereas the high electronic conductivity provides superhighways for electron transportation, therefore enhancing the cycling stability at large current densities [87]. Dai et al. used 3D graphene foams, which were fabricated by CVD process at 1000 °C, as cathode material for AIBs with a high electrochemical performance [8]. The foams afforded charging times of around 1 min with a current density of ~4,000 mA g^{-1} (equivalent to ~3,000 W kg^{-1}) and withstood more than 7,500 cycles without capacity decay. Yu et al. prepared monolithic nanoporous graphene foam by annealing GO at 1050 °C to improve the performance of AIBs, demonstrating a volumetric capacity of 12.2 mAh cm^{-3} and a gravimetric capacity of 151 mAh g^{-1} [88]. Gao et al. prepared a 3D GA by graphitizing GO at 3000 °C to increase the capacity of AIBs, affording a high capacity of 100 mAh g^{-1} under an ultrahigh rate of 500 C [1]. High synthesis temperatures result in high energy consumption and cost, which are not conducive to the manufacture of green and low-cost AIBs. In this context, we discuss the recent progress in carbon electrodes with different features (Fig. 10) based on various energy storage devices to provide practical guidance for the design of low-cost AIBs.

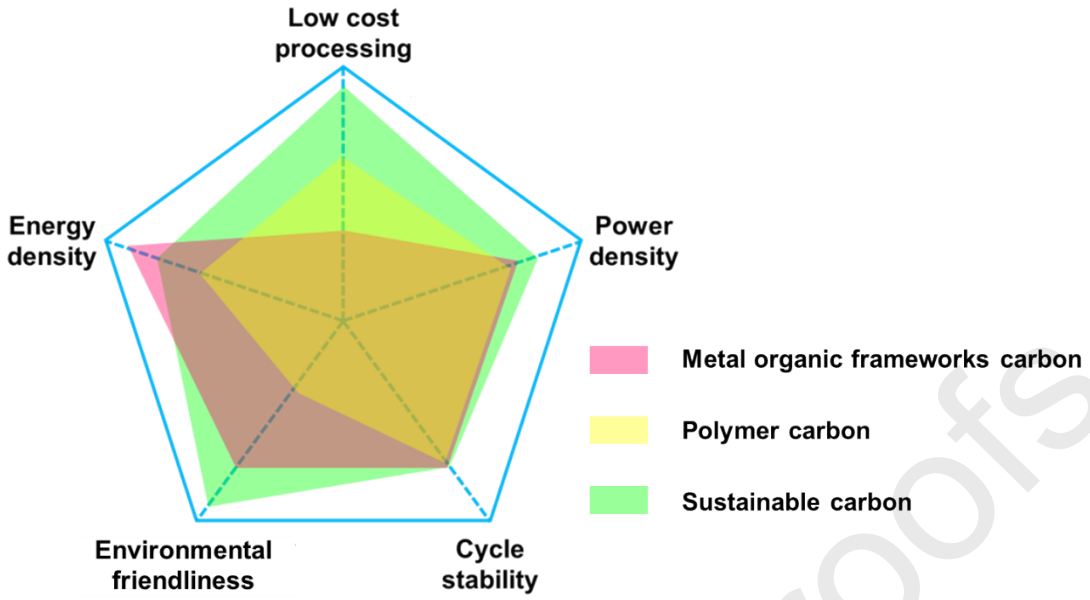

Fig. 10 Feature comparison of MOFs, polymers, and sustainable carbons.

Table 3 Electrochemical performance of carbon materials prepared by different methods

Classification	Carbon	Precursor	Annealed temperature (°C)	Specific surface area ($m^2 g^{-1}$)	Device (Anode|electrolyte|cathode)	Electrochemical performance			Ref.
						Capacity	At highest current density	Cycle life	
MOF-based carbon	N-doped wrinkled carbon foils	Mn-MOF (1,4-benzenedicarboxylic acid)	600	417.8	Na|1 M $NaClO_4$ in EC/PC|carbon	306 mA h g^{-1} at 0.05 A g^{-1}	150 mAh g^{-1} at 10 A g^{-1}	A capacity retention of 72.8% after 1000 cycling at 1.0 A g^{-1}	[89]
	NCPPs/g-CN	Zn-ZIF-8 (2-methylimidazole)	800	453.5	Carbon|1 M H_2SO_4|carbon	495 F g^{-1} at 0.1 A g^{-1}	188 F g^{-1} at 20 A g^{-1}	No capacitance declination after 2500 cycles at 10 A g^{-1}	[90]
	ZIF-8@PZS-C	Zn-ZIF-8 (2-methylimidazole)	900	929	Graphite|0.5 M NaCl|carbon	333 F g^{-1} at 1 mV s^{-1}	-	No capacitance declination after 10000 cycles at 10 A g^{-1}	[91]
Polymer-based carbon	Carbon aerogels	Polymerization of phenol–formaldehyde	800	1340	Li|1 M $LiPF_6$ in EC/DMC|carbon	798.2 mAh g^{-1} at 0.1 A g^{-1}	190 mAh g^{-1} at 2 A g^{-1}	300 mAh g^{-1} after 1000 cycles at 1.0 A g^{-1}	[92]
	N-and P-co-doped carbon hollow spheres	Dehydrated polypyrrole	800	1155	Carbon|6 M KOH|carbon	232 F g^{-1} at 1 A g^{-1}	170 F g^{-1} at 10 A g^{-1}	89.1% capacitance after 5000 cycles at of 5 A g^{-1}.	[93]
	N-and O-co-doped carbon foam	Quinone–amine polymer	750	1215	Carbon|1 M H_2SO_4|carbon	410 F g^{-1} at 1 A g^{-1}	275 F g^{-1} at 50 A g^{-1}	98% capacitance after 15000 cycles at 5 A g^{-1}	[94]
	N-doped carbon	N-doped benzene	800	1252	Carbon|1 M H_2SO_4|carbon	295 F g^{-1} at 0.1 A g^{-1}	-	81% capacitance after 15000 cycles at 10 A g^{-1}.	[95]
	N-enriched porous carbon	Polymer-silica hybrid polymerized high internal phase emulsions	900	1150	Carbon|1 M H_2SO_4|carbon	209 F g^{-1} at 1 A g^{-1}	176 F g^{-1} at 20 A g^{-1}	83% capacity retention after 5000 cycles at 10 A g^{-1}	[96]
Bio-based carbon	Cashewnut sheath carbon	Cashewnut sheath	800	1967	Lithium ion battery	721 mAh g^{-1} at 0.1 A g^{-1}	280 mAh g^{-1} at 1 A g^{-1}	271 mAh g^{-1} at 0.5 mA g^{-1} after 200 cycles	[97]
					Sodium ion battery	200 mAh g^{-1} at 0.1 A g^{-1}	55 mAh g^{-1} at 5 A g^{-1}	55 mAh g^{-1} at 5 A g^{-1} after 300 cycles	

Graphene bio-carbon xerogel	Cellulose	800	2994	Carbon|6 M KOH|carbon	189 F g^{-1} at 1 A g^{-1}	139 F g^{-1} at 100 A g^{-1}	100% capacity retention after 10000 cycles at 5 A g^{-1}.	[98]
S-doped micro/mesoporous bio-carbon	Lignin	850	660	Carbon|1 M KOH|carbon	225 F g^{-1} at 0.5 A g^{-1}	195 F g^{-1} at 10 A g^{-1}	100% capacity retention after 10000 cycles at 5 A g^{-1}.	[99]
Corn silk-derived carbon	Corn silk	800	2550	Na|1 M $NaClO_4$|carbon	256 mAh g^{-1} at 0.1 A g^{-1}	45 mAh g^{-1} at 20 A g^{-1}	73.3% capacity retention after 1000 cycles at 1 A g^{-1}.	[100]
Honeycomb-like porous carbons	Aloe peel	800	1286	Carbon|I_3^-/I^- electrolyte |carbon	264 F g^{-1} at 0.5 A g^{-1}	204.5 F g^{-1} at 30.0 A g^{-1}	91% capacitance retention after 5000 cycles at 0.5 A g^{-1}	[101]
N-S-P-O co-doped carbon foams	Waste-fish bones	900	1670	Li|1 M $LiPF_6$ in EC/DMC|carbon	160 mAh g^{-1} at 0.1 A g^{-1}	32 mAh g^{-1} at 50 A g^{-1}	58 mAh g^{-1} at 5 A g^{-1} after 10000 cycles	[102]

1

4.1 MOF-based carbon

MOFs are a porous crystalline material formed by covalent bonding of metal ions and organic ligands and usually have a regular polyhedral morphology [103-105]. Pyrolysis of MOFs under an inert atmosphere is an effective method for preparing porous carbon materials with a certain degree of graphitization [106-108]. Such carbon materials exhibit excellent performance in energy storage due to the ordered porosity and high electronic conductivity [109-111].

Kong et al. [89] demonstrated the synthesis of N-doped wrinkled carbon foils with multiscale pore architecture (a specific surface area of 417.8 m^2 g^{-1}) and abundant N species through the synthesis and pyrolysis of 2D MOFs and a subsequent acid etching process (Fig. 11a). In sodium-ion capacitors, the carbon foil delivered a capacity of 150 mA h g^{-1} at 10 A g^{-1} (Fig. 11b) and a capacity retention of 72.8% after 1000 cycling at 1.0 A g^{-1} (Fig. 11c). To improve ion transportation and faradic reactions during the charge–discharge process, Kong et al. [90] developed a ZIF-8-derived N-doped carbon polyhedral particles (NCPPs) with a hierarchically porous structure (specific surface area of 453.5 m^2 g^{-1}) and a high nitrogen doping (25.06 at%) decorated on graphitic carbon nitride (g-CN) composite electrode materials (NCPPs/g-CN, Fig. 11d). The electrode displayed specific capacitances of 349.7 and 261.2 F g^{-1} at 0.5 and 5 A g^{-1}, respectively (Fig. 11e), and a stable cycle performance with no capacitance declination after 2500 cycles at 10 A g^{-1}.

Heterogeneous atom doping and morphological structure design also play important roles in the preparation of MOF-based carbon materials. Zhang et al. [91]

synthesized N, P, and S co-doped hollow carbon polyhedrons with a hollow structure, a surface area of 929 m^2 g^{-1}, and excellent hydrophilic surface, which were derived from poly (cyclotriphosphazene-co-4,4'-sulfonyldiphenol)-coated zeolitic imidazolate framework-8 (ZIF-8@PZS-C) through pyrolysis (900 °C) and acid etching processes. Given the above multi-synergy, the ZIF-8@PZS-C electrodes achieved a specific capacitance of 333 F g^{-1} at 1 mV s^{-1} (Fig. 11f) and a cycling stability without evident change after 10000 cycles at 10 A g^{-1} (Fig. 11g). For the research of MOF-based carbon electrode, our group [112] reported a synthesis approach for graphitized mesoporous carbons (GMCs) derived from ZIF-8 via controlling the annealing parameters. The GMC with a specific surface area of 430.63 m^2 g^{-1} improved the cycle life of lead acid battery from 4408 cycles to 38013 cycles and enhanced the capacity retention of lithium anode (0.5 C and 200 cycles) from 42.3% to 90.1%. Moreover, we demonstrated that carbon materials derived from MOFs possess a good potential for energy storage through the modification of $LiFePO_4$/carbon cathode materials [113-115]. These studies lay the foundation for applications of MOF-based carbon materials in batteries.

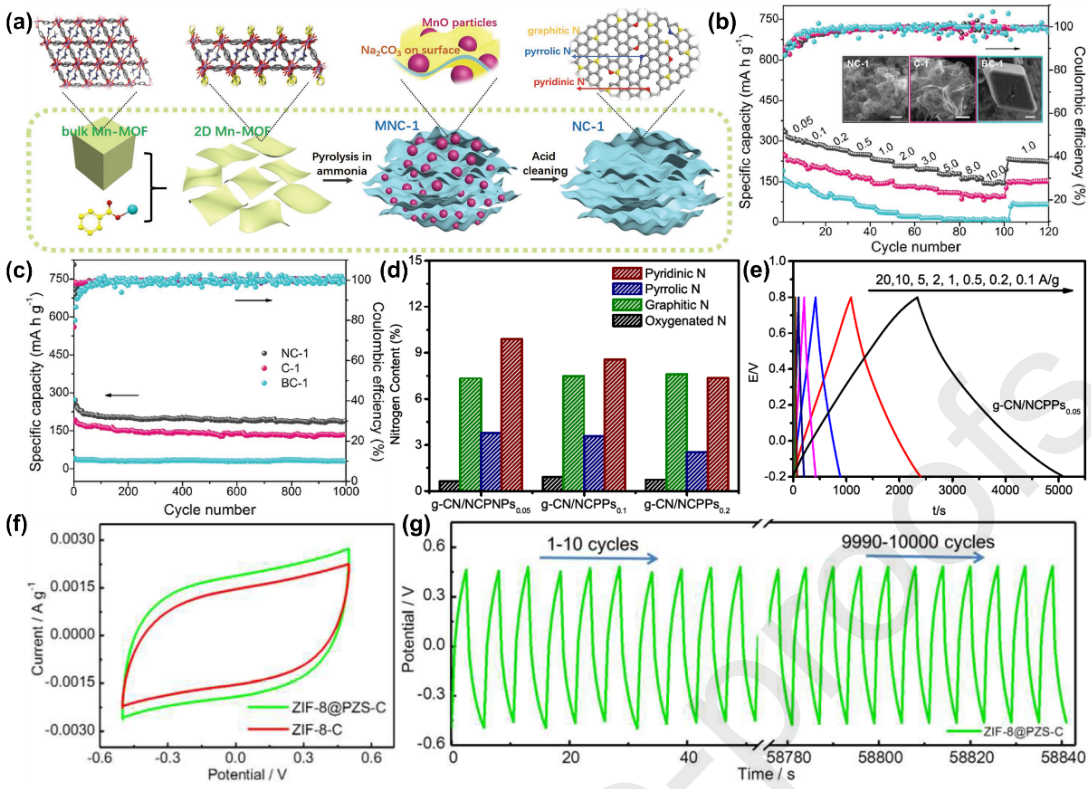

Fig. 11 (a) Schematic of the formation process of NC-1 from bulk Mn-MOF. (b) Rate capabilities of NC-1, C-1, and BC-1. (c) Cycling performances of NC-1, C-1, and BC-1 at a current density of 1.0 A g^{-1} [89]. Copyright 2018, Wiley. (d) Contents of different nitrogen configurations in g-CN/NCPPs$_{0.05}$, g-CN/NCPPs$_{0.1}$, and g-CN/NCPPs$_{0.2}$. (e) Charge–discharge curves of g-CN/NCPPs$_{0.05}$-based electrodes at different current densities [90]. Copyright 2018, Elsevier. (f) Cyclic voltammograms of ZIF-8-C and ZIF-8@PZS-C at a scan rate of 1 mV s^{-1}. (g) galvanostatic charge-discharge (GCD) cycles curves of the first and last 10 cycles (from 9990th cycle to 10000th cycle) at 10 A g^{-1} [91]. Copyright 2018, Royal Society of Chemistry.

4.2 Polymer-based carbon

Although annealing MOFs in an inert atmosphere can obtain a carbon material with superior electrochemical performance and provide a positive reference for high-

power-density AIBs, the high cost of MOF raw material and low yield are not conducive to large-scale application of AIBs [113, 116, 117]. The pyrolysis of polymers under inert atmosphere has a significant cost advantage in the preparation of carbon materials [116, 118-122]. Woodward et al. [123] reported the carbonization of poly(divinyl benzene) high internal phase emulsions (HIPEs) (produced by polymerization of rGO-stabilized HIPEs) to produce carbo-HIPEs possessing a specific surface area of 1820 $m^2 g^{-1}$, an electrical conductivity of 285 S m^{-1}, and a power density of 280 W kg^{-1}. Yu et al. [92] reported a route to produce CAs with a low density of about 25 mg cm^{-3} and a specific surface area of 1340 $m^2 g^{-1}$ based on polymerization of PF under hypersaline conditions at 800 °C. The CA provided a capacity of 798.2 mAh g^{-1} at 0.1 A g^{-1}, and a capacity of 427 mAh g^{-1} was retained after 100 cycles in lithium ion battery.

Heteroatom doping is an important approach to improve the performances of carbon-based electrode materials in energy storage and conversion field. Lv et al. [93] prepared N- and P-co-doped carbon hollow spheres (NPCHSs) by carbonization of dehydrated polypyrrole hollow spheres and subsequent KOH activation. High-level heteroatom doping with N (11.4 wt%), O (6.7 wt%), and P (3.5 wt%) was obtained in NPCHS carbon, exhibiting a specific surface area of 1155 $m^2 g^{-1}$, a high specific capacitance of 232 F g^{-1} at 1 A g^{-1}, and a retention of 89.1% after 5000 cycles at 5 A g^{-1}. Zhang et al. [94] developed a strategy based on the design of faradaic redox active sites to synthesize N- and O-co-doped carbon foam with a hierarchical porous structure by a facile two-step method of incipient impregnation and carbonization (Fig. 12a). The

obtained carbon foam possessed a high content of heteroatoms (total N and O 12.26 at%), and its hierarchical porous structure provided a specific surface area of 1215 m^2 g^{-1}. In a symmetrical supercapacitor, the foam delivered a specific capacitance of 321 F g^{-1} at 1 A g^{-1}, an energy density of 15.91 Wh kg^{-1} at the power density of 0.4 kW kg^{-1} (Fig. 12b), and good stability of the remaining 98% capacitance after 15000 cycles at 5 A g^{-1}.

Carbonization of hypercrosslinked polymers can be used to generate conductive carbons using low-cost precursors while allowing heteroatoms to be incorporated by the choice of feedstock and by changing the type of gas used in carbonization. Lee et al. [95] reported that N-doped benzene annealed at 800 °C possessed an N content of 7.5 wt%, a specific surface area of 1252 m^2 g^{-1}, and a capacitance of 295 F g^{-1} at 0.1 A g^{-1} with an excellent capacitance retention of 81% at 10 A g^{-1}. Deshmukh et al. [96] synthesized NPC nanosheets by pyrolysis of polymer-silica hybrid with internal phase emulsion methodology (polyHIPE) and subsequent silica removal (Fig. 12c). The material annealed at 900 °C possessed a micro/meso hierarchical porous structure with a specific surface area of 1150 m^2 g^{-1}. This NPC (2.7 at%) showed a good rate capability (84% capacitance retention at 20 A g^{-1}, a high specific capacitance of 209 F g^{-1} at 1 A g^{-1}, and long cycling stability (83% capacity retention after 5000 cycles at 10 A g^{-1}, Fig. 12d).

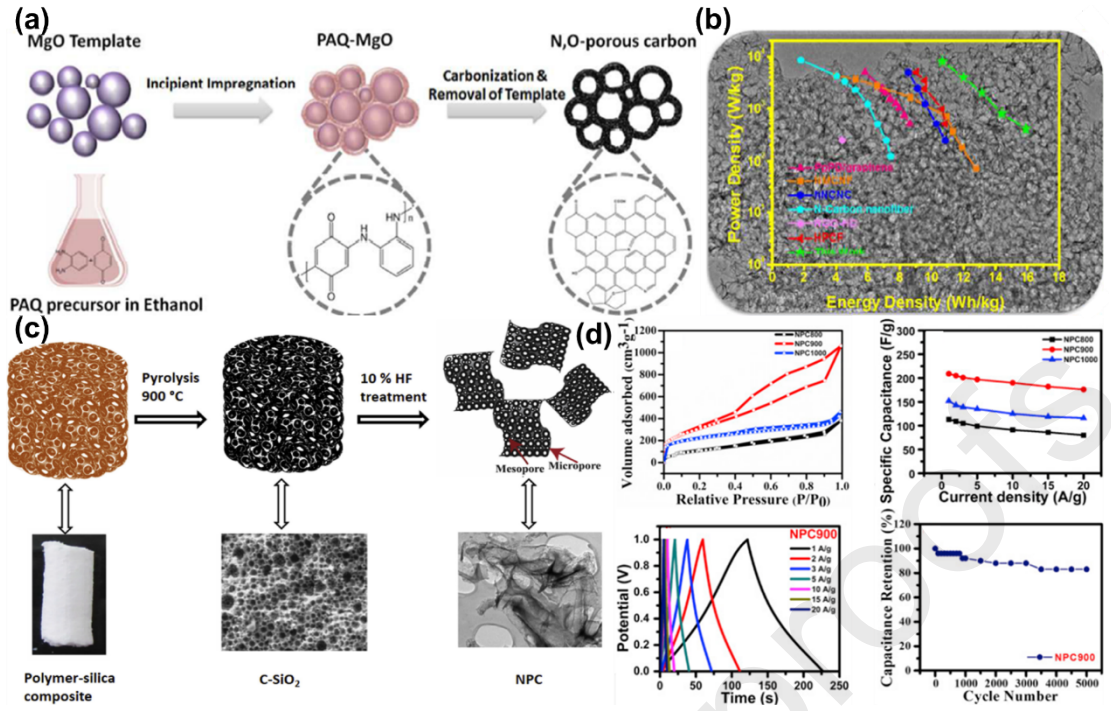

Fig. 12 (a) Schematic showing the synthesis of porous nitrogen and oxygen-doped carbon foam via a PAQ precursor by an incipient wetness impregnation and subsequent carbonization. (b) Transmission electron microscopy image and the N,O-PCF750-based symmetrical supercapacitor performance in 1 M H_2SO_4 and 1 M Li_2SO_4 electrolyte compared with references [94]. Copyright 2018, Royal Society of Chemistry. (c) Schematic of the formation process for NPC from polymer silica hybrid polyHIPE material. (d) N_2 adsorption–desorption isotherms for NPC 800, NPC900, and NPC1000; Specific capacitances of NPC800, NPC900, and NPC1000 at different current densities; Charge–discharge curves of NPC900 at different current densities in 1 M H_2SO_4; Cycle performance of NPC900 at current density of 10 A g^{-1} for 5000 cycles [96]. Copyright 2018, Elsevier.

4.3 Sustainable carbon

Polymer-based carbon materials can significantly reduce cost and increase yields

compared with MOF-based carbon materials. However, polymer preparation usually requires additives and initiators, which can cause environmental pollution [124, 125]. Nature is the greatest factory in the world with green and pollution-free features, producing various biomaterials with complicated, elaborate, and efficient hierarchical morphologies and multiple nanoscale assemblies to satisfy specific requirements of the preparation of energy storage materials [126-128]. Moreover, biomaterials usually contain elements, such as carbon, hydrogen, oxygen, nitrogen, phosphorus, and sulfur, which enable the in-situ preparation of atom-doped carbon materials [129-131]. Nagalakshmi et al. [97] synthesized CNSC with a high surface area of 1967 $m^2 g^{-1}$ and a conductivity of 0.1638 mS cm^{-1} through carbonization of cashewnut sheath at 800 °C, followed by KOH activation. The CNSC delivered capacities of 620 mAh g^{-1} at 0.1 A g^{-1} and 271 mAh g^{-1} at 0.5 mA g^{-1} in lithium ion batteries and 200 mAh g^{-1} at 0.1 A g^{-1} and 55 mAh g^{-1} at 5 A g^{-1} in sodium ion batteries. Yang et al. [98] fabricated a graphene-functionalized bio-carbon xerogel with a specific surface area of 2994 $m^2 g^{-1}$ and a pore volume of 1.8 $cm^3 g^{-1}$ derived from cellulose for supercapacitor. The bio-carbon xerogel retained 100% of the initial specific capacitance after 10000 cycles at 5 A g^{-1}. Demir et al. [99] synthesized a sulfur self-doped carbon material from lignin via hydrothermal carbonization followed by thermal annealing. The as-prepared sulfur self-doped carbon at 850 °C exhibited a specific surface area of 660 $m^2 g^{-1}$ with abundant micro/meso porous structure and demonstrated a capacity of 225 F g^{-1} at 0.5 A g^{-1} and high durability up to 10000 cycles at 5 A g^{-1}.

Vadivazhagan et al. [100] synthesized a porous carbon through pre-carbonization

at 800 °C and KOH activation of corn silk (Fig. 13a), possessing a specific surface area of 2550 $m^2 g^{-1}$ and a pore volume of 0.95 $cm^3 g^{-1}$. The porous carbon exhibited specific capacities of 256, 212, 159, 126, 84, 53, and 35 mAh g^{-1} at 0.1, 0.2, 0.5, 1, 2, 5, and 10 A g^{-1} in sodium ion battery, respectively (Fig. 13b). Wang et al. [101] prepared aloe peel-derived honeycomb-like porous carbons (AP-HC) with a specific surface area of 1286 $m^2 g^{-1}$ by combining simple hydrothermal carbonization with chemical activation (Fig. 13c). In supercapacitors, a high retention rate of ~77.45% (ranging from 0.5 A to 30.0 A g^{-1}, Fig. 13d) and superior cycling performance (91% capacitance retention after 5000 cycles, Fig. 13e) were demonstrated. Shan et al. [102] fabricated a naturally fibrous carbon foam with a surface area of 1670 $cm^2 g^{-1}$ and a pore volume of 3.86 $cm^3 g^{-1}$ by employing a food waste–fish bone as raw materials (Fig. 13f). N-S-P-O co-doping was achieved in the carbon foams. Benefiting from the synergistic effects of hierarchically porous fibrous foam and multiple heteroatom doping, the foam delivered a power density of 62 kW kg^{-1} and an energy density of 72 Wh kg^{-1}. As shown in Fig. 13g, the current densities can reach up to 50 A g^{-1}, indicating the material's superior high rate performance. At 5 A g^{-1} for 10000 cycles, the foam can retain a capacity of 58 mAh g^{-1} (Fig. 13h).

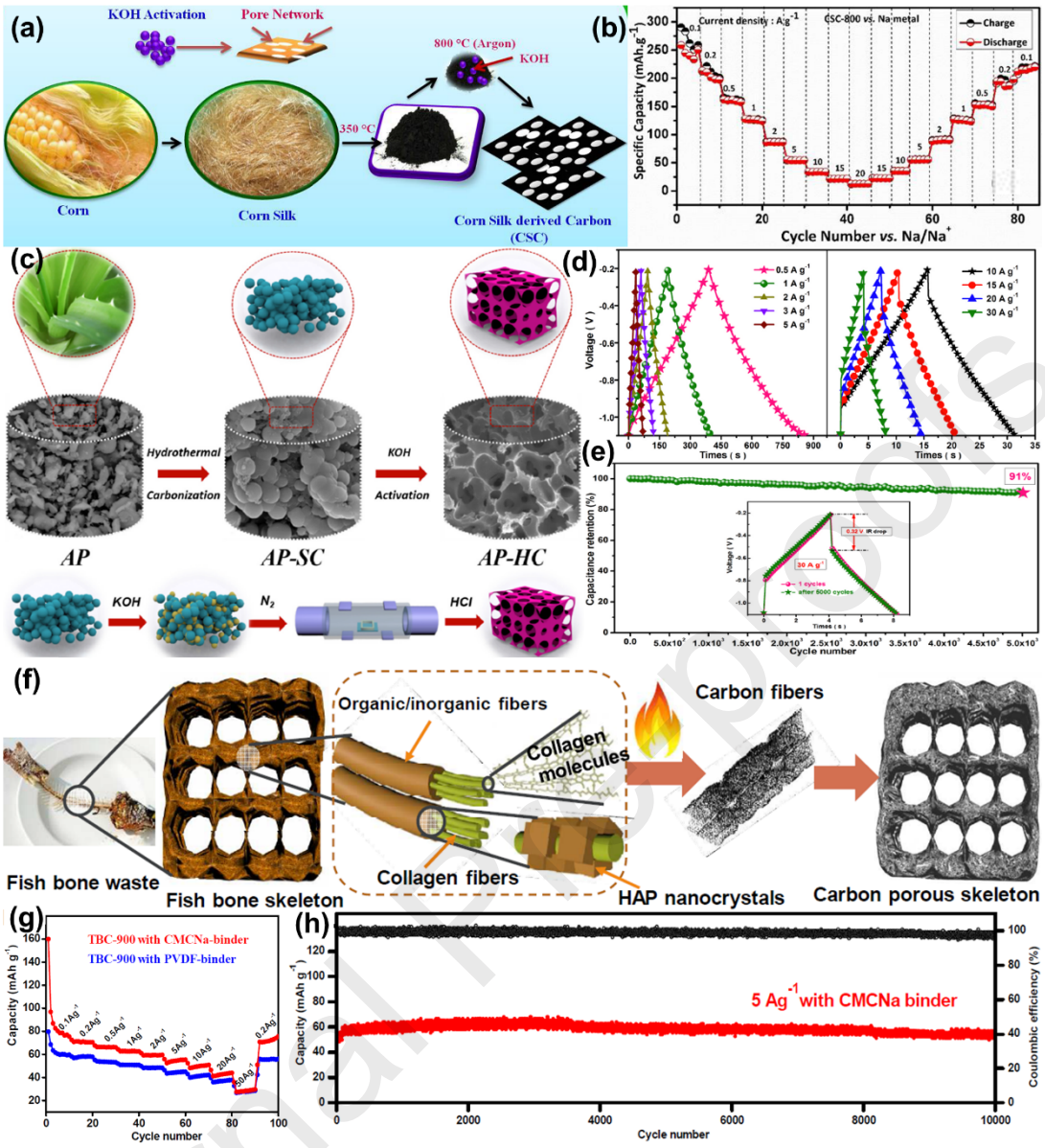

Fig. 13 (a) Schematic of synthesis of CSC. (b) Rate capability studies of CSC electrode [100]. Copyright 2018, American Chemical Society. (c) Schematic of the synthesis and controllable morphology transformation of bio-based carbon materials (AP: aloe peel, SC: spherical carbon, and HC: honeycomb-like carbon). Electrochemical performance of the AP-HC material tested using a three-electrode system in 6 M KOH electrolyte: (d) GCD curves of AP-HC at various current densities from 0.5 A g^{-1} to 30 A g^{-1}; (e) cycling stability of AP-HC electrode at 30 A g^{-1} (inset: charge–discharge curves before and after 5000 cycles) [101]. Copyright 2019, Elsevier. (f) Schematic of the

microstructural change from fish bones to tuna bones carbons (TBCs). (g) Rate comparison of TBC-900 cathodes with CMCNa and polyvinylidene difluoride binders. (h) Cycling performance of CMCNa-binder TBC-900 cathode [102]. Copyright 2019, American Chemical Society.

5 Perspective on AIBs

We will provide our perspectives on the rational design of high-performance AIBs in accordance with the requirements of practical applications (Fig. 14). Anode, cathode, electrolyte, and cell design will be discussed in detail.

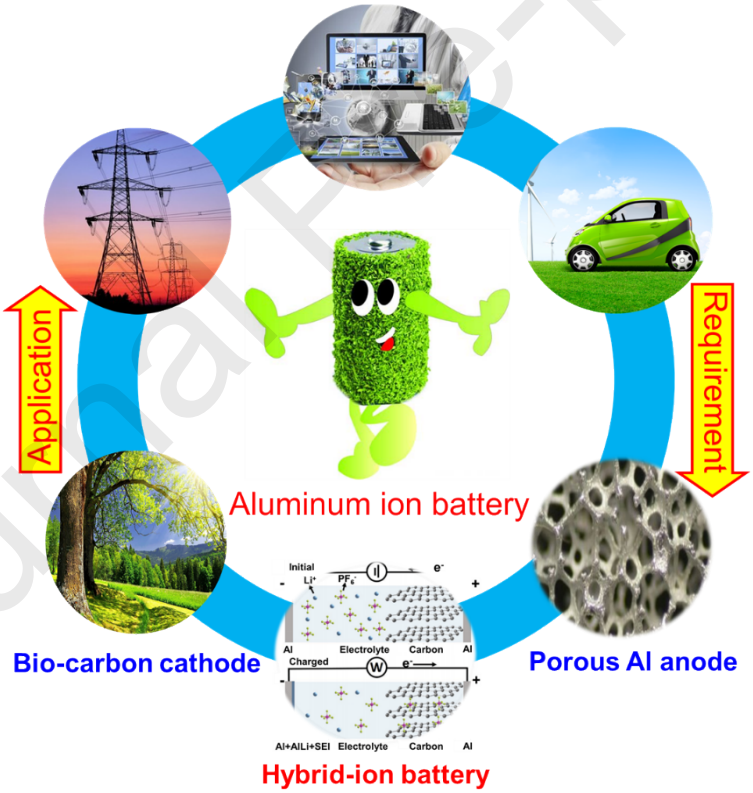

Fig. 14 Perspective: design and configuration of high-performance AIBs for practical applications.

5.1 Anode

Increasing the specific surface area by reducing the dimension and designing a proper pore structure benefit the enlargement of the interface of chemical reactions [132, 133]. Al foam, porous Al, and Al powder have become effective approaches to improve the electrochemical reaction activity of Al anodes. Furthermore, the high surface specific area can balance the distribution of electrons on the surface of Al anode, and the growth of Al dendrite can be effectively suppressed during the discharge process. In general, Al powder possesses a higher specific surface area with a lower cost than porous Al [134, 135]; thus, Al powder anode can be the most potential candidate of high-power AIBs.

For powdery materials, the route for the preparation and formation of electrode plate plays an important role in electrochemical performance. Tong et al. [39] used Al nanosphere as active material for AIBs; the binder was necessary in the preparation process of the electrode plate. The presence of binder may limit the advantage of powdery anode; binder-free metal powdery electrode plate will be the focus in AIB anodes. We propose two ways to prepare binder-free Al electrode based on other battery systems: (1) referencing the preparation of metal Li powder electrode plate with a high electrochemical performance [136, 137]; (2) referencing the negative electrode of lead acid battery systems [112, 138]. The Al powder anode can be prepared via the processes of Al paste preparation, and the Al paste can be coated on the Al network, followed by dry solidification and final electrochemical formation.

5.2 Cathode

Different from anodes, various types of cathode active materials, such as chloride, sulfide, sulfur, Prussian blue, polyanion, vanadium oxide, polymers, halogen and carbon, exist, as summarized by Zhang's group [18]. Based on the recent processes of AIBs, we summarize the three types of materials, such as carbon, metal compound and composite types. Table 2 indicates that carbon materials possess a high rate (high current density) performance and cycle life, whereas metal compounds have the highest discharge specific capacities and the poorest cycle life. The composites consist of carbon materials and metal compounds with an enhanced cycle life and low high-rate performance. Therefore, carbon materials can be the choice for the fabrication of high-power AIBs.

The preparation approach of carbon materials significantly affects the production costs of AIBs, and the degree of graphitization plays an important role in high power density. Various methods for preparing functional carbon materials, such as CVD, sol-gel method, solvothermal method, and freeze drying, have been proposed [116, 117]. Direct carbonization of organic materials may be the best choice due to their simple process and low energy consumption [138, 139]. We summarize the approaches for preparing graphitized carbon material, such as MOF-based carbon, polymer-based carbon and bio-based carbon based on the recent processes of carbon matrix electrodes. The high cost of MOFs limits their large-scale production, and the pollution of polymer preparations, which are only suitable to studies in the laboratory, cannot match the goal of green production. The bio-based carbon is derived from natural products with the

advantages of being green, non-pollution, and cheap. Furthermore, natural products possess rich structures and ordered pores, which are beneficial to the design of a carbon matrix with good physical and chemical properties. The design and preparation of bio-carbon derived from natural products, such as leaves, wood, grass, cell of fruit/nut, skin and hair of animals, etc., maybe an effective route to obtain a low-cost carbon cathode for AIBs. The preprocessing of natural products, such as acidification, alkali wash, freeze drying, and diacylation, should be further studied to reach high electrochemical performance.

5.3 Electrolyte and cell design

The electrolyte of AIBs is important during charge and discharge processes. Based on the differences among electrolytes, battery cell designs can be divided into three categories: traditional, hybrid, and all-solid-state AIBs. For traditional AIBs, the type of effective liquid electrolyte is limited. $AlCl_3$ has been identified as a metal salt. Meanwhile, the search for organic solution and additives is the most challenging in future research. In addition, the exploration of safe and inexpensive aqueous electrolytes will be another development direction for AIBs [140]. The dual ionic AIBs obtained by utilizing 4.0 M $LiPF_6$ as electrolyte in ethyl methyl carbonate offers a constructional suggestion for hybrid AIBs, in which effective ion exchange plays a great role in the enhancement of AIB performance. The exploration of other electrolyte systems should be performed from the perspective of other systems [141, 142], such as sodium [143], zinc [20], magnesium [144], and calcium ion batteries[145, 146].

Moreover, the effect of ionic size on ionic exchange should be the research focus for high-performance hybrid AIBs. In all-solid-state and flexible energy storage systems, the solid-state electrolyte is an important branch. Wang et al. [147] investigated the phosphate-type solid-state electrolyte $(Al_{0.2}Zr_{0.8})_{20}/_{19}Nb(PO_4)_3$ for rechargeable solid-state AIBs. The Al|$(Al_{0.2}Zr_{0.8})_{20}/_{19}Nb(PO_4)_3$|$V_2O_5$ nanorods/rGO cell showed the initial discharge capacities of 7.5 and 10 mAh·g^{-1} at 120 °C and 150 °C, respectively, from 0.01 V to 2.0 V versus Al^{3+}/Al at 2 mA g^{-1}. This research opens the way for the study of solid-state AIBs. The development of other inorganic solid-state electrolytes and the exploration of flexible solid-state electrolytes display importance for high-power density and low-cost AIBs.

6 Conclusion

In summary, global energy crisis and environmental pollution from fossil fuels have aroused widespread interest in the development of high-performance energy storage systems that can be integrated with intermittent renewable energy sources. AIBs for electrochemical energy storage technologies received considerable attention because of the advantages of high theoretical specific capacity, lightweightness, zero pollution, safety, low cost, and rich resource. Especially, the potential of ultra-fast charge and discharge caused by three-electron redox reactions paves the way for next-generation high-power rechargeable batteries.

Based on the principles of AIBs, the challenges for different components, such as anode, electrolyte, and cathode, were reviewed. For the research focus and bottleneck

of AIBs, we comprehensively discussed the preparation of green and low-cost carbonaceous cathode materials with high performance based on existing electrode materials. Various perspectives, including anode design and protection, electrolyte exploitation and modification, and cathode selection and preparation, were proposed. As a promising battery technology, AIB production presents enormous opportunities and challenges. Extra efforts are necessary for the (1) development of simple but effective approaches for the synthesis and treatment of bio-carbon matrix for cathodes with excellent electrochemical performance; (2) exploration of other types of low-cost electrolyte for the production of large-scale AIBs; (3) design of optimized anode structure (increased specific surface area) to enhance the dissolution/deposition kinetics of the anode and suppress Al dendrite growth. AIBs are expected to be developed as competitive technologies for energy storage and as a solution for various energy-related challenges. Nevertheless, future development in AIBs should offer new insights into the achievement of such goals.

Acknowledgement: This work was supported by the funding from Qilu University of Technology, the 2020 Major Engineering Project of New and Old Kinetic Energy Conversion of Shandong Province (Research and Industrialization of Key Common Technologies for Efficient Preparation of Lithium Battery Separators with Excellent Temperature Resistance), the National Natural Science Foundation of China (51972180 and 51572134), the Key Technology Research and Development Program of Shandong (2019GGX102070), the Program for Scientific Research Innovation Team in Colleges and Universities of Jinan (2018GXRC006), the Science and Technology Development Fund, Macau SAR (File no. 191/2017/A3, 041/2019/A1, 201/2019/AIR, 046/2019/AFJ), the Multi-Year Research Grants (MYRG2017-00216-FST and MYRG2018-00192-IAPME) from the Research Services and Knowledge Transfer Office at the University of Macau, and UEA funding.

References

[1] H. Chen, F. Guo, Y. Liu, T. Huang, B. Zheng, N. Ananth, Z. Xu, W. Gao, C. Gao, A Defect-Free Principle for Advanced Graphene Cathode of Aluminum-Ion Battery, Adv. Mater. 29 (2017) 1605958.

[2] Y. Wu, M. Gong, M.C. Lin, C. Yuan, M. Angell, L. Huang, D.Y. Wang, X. Zhang, J. Yang, B.J. Hwang, H. Dai, 3D Graphitic Foams Derived from Chloroaluminate Anion Intercalation for Ultrafast Aluminum-Ion Battery, Adv. Mater. 28 (2016) 9218-9222.

[3] X. Zhang, Y. Tang, F. Zhang, C.S. Lee, A Novel Aluminum-Graphite Dual-Ion Battery, Adv. Energy Mater. 6 (2016) 1502588.

[4] H. Li, X. Zhang, Z. Zhao, Z. Hu, X. Liu, G. Yu, Flexible sodium-ion based energy storage devices: Recent progress and challenges, Energy Storage Mater. 26 (2020) 83-104.

[5] L. Zhang, K.N. Hui, K. San Hui, H. Lee, High-performance hybrid supercapacitor with 3D hierarchical porous flower-like layered double hydroxide grown on nickel foam as binder-free electrode, J. Power Sources 318 (2016) 76-85.

[6] L. Zhang, K.N. Hui, K.S. Hui, H. Lee, Facile synthesis of porous CoAl-layered double hydroxide/graphene composite with enhanced capacitive performance for supercapacitors, Electrochim. Acta 186 (2015) 522-529.

[7] L. Li, K.S. Hui, K.N. Hui, Y.R. Cho, Ultrathin petal-like NiAl layered double oxide/sulfide composites as an advanced electrode for high-performance asymmetric supercapacitors, J. Mater. Chem. A 5 (2017) 19687-19696.

[8] M.C. Lin, M. Gong, B. Lu, Y. Wu, D.Y. Wang, M. Guan, M. Angell, C. Chen, J. Yang, B.J. Hwang, H. Dai, An ultrafast rechargeable aluminium-ion battery, Nature 520 (2015) 325-328.

[9] Y. Hu, D. Ye, B. Luo, H. Hu, X. Zhu, S. Wang, L. Li, S. Peng, L. Wang, A Binder-Free and Free-Standing Cobalt Sulfide@Carbon Nanotube Cathode Material for Aluminum-Ion Batteries, Adv. Mater. 30 (2018) 1703824.

[10] H. Yang, H. Li, J. Li, Z. Sun, K. He, H.M. Cheng, F. Li, The Rechargeable Aluminum Battery: Opportunities and Challenges, Angew. Chem. 58 (2019) 11978-11996.

[11] J. Tu, M. Wang, X. Xiao, H. Lei, S. Jiao, Nickel Phosphide Nanosheets Supported on Reduced Graphene Oxide for Enhanced Aluminum-Ion Batteries, ACS Sustainable Chem. Eng. 7 (2019) 6004-6012.

[12] S. Kumar, R. Satish, V. Verma, H. Ren, P. Kidkhunthod, W. Manalastas, M. Srinivasan, Investigating $FeVO_4$ as a cathode material for aqueous aluminum-ion battery, J. Power Sources 426 (2019) 151-161.

[13] Y. Hu, Y. Bai, B. Luo, S. Wang, H. Hu, P. Chen, M. Lyu, J. Shapter, A. Rowan, L. Wang, A Portable and Efficient Solar-Rechargeable Battery with Ultrafast Photo-Charge/Discharge Rate, Adv. Energy Mater. 9 (2019) 1900872.

[14] D. Ye, B. Luo, G.M. Lu, L. Wang, Will new aluminum-ion battery be a game changer?, Sci. Bull. 60 (2015) 1042-1044.

[13] Y. Hu, D. Sun, B. Luo, L. Wang, Recent Progress and Future Trends of Aluminum Batteries, Energy Technology 7 (2019) 86-106.

[16] Z. Hu, H. Zhang, H. Wang, F. Zhang, Q. Li, H. Li, Nonaqueous Aluminum Ion Batteries: Recent Progress and Prospects, ACS Mater. Lett. 2 (2020) 887-904.

[17] Z. Zhao, Z. Hu, Q. Li, H. Li, X. Zhang, Y. Zhuang, F. Wang, G. Yu, Designing two-dimensional WS_2 layered cathode for high-performance aluminum-ion batteries: From micro-assemblies to insertion mechanism, Nano Today 32 (2020) 100870.

[18] Y. Zhang, S. Liu, Y. Ji, J. Ma, H. Yu, Emerging Nonaqueous Aluminum-Ion Batteries: Challenges, Status, and Perspectives, Adv. Mater. 30 (2018) e1706310.

[19] S. K. Das, Graphene: A Cathode Material of Choice for Aluminum-Ion Batteries, Angew. Chem. Int. Ed. 57 (2018) 16606-16617.

[20] V. Verma, S. Kumar, W. Manalastas, R. Satish, M. Srinivasan, Progress in Rechargeable Aqueous Zinc- and Aluminum-Ion Battery Electrodes: Challenges and Outlook, Adv. Sustain. System. 3 (2019) 1800111.

[21] P. Bilski, B. Marczewska, Fluorescent detection of single tracks of alpha particles using lithium fluoride crystals, Nuclear Instruments and Methods in Physics Research Section B: Beam Interactions with Materials and Atoms 392 (2017) 41-45.

[22] Y. Gao, C. Zhu, Z. Chen, G. Lu, Understanding Ultrafast Rechargeable Aluminum-Ion Battery from First-Principles, J. Phy. Chem. C 121 (2017) 7131-7138.

[23] F. Wu, H. Yang, Y. Bai, C. Wu, Paving the Path toward Reliable Cathode Materials for Aluminum-Ion Batteries, Adv. Mater. 31 (2019) e1806510.

[24] X. Xu, S. Wang, H. Wang, C. Hu, Y. Jin, J. Liu, H. Yan, Recent progresses in the suppression method based on the growth mechanism of lithium dendrite, J. Energy Chem. 27 (2018) 513-527.

[25] X. Xu, K.S. Hui, D.A. Dinh, K.N. Hui, H. Wang, Recent Advances in Hybrid Sodium-Air Batteries, Mater. Horiz. 6 (2019) 1306-1335.

[26] H. Chen, H. Xu, B. Zheng, S. Wang, T. Huang, F. Guo, W. Gao, C. Gao, Oxide Film Efficiently Suppresses Dendrite Growth in Aluminum-Ion Battery, ACS Appl. Mater. Interfaces 9 (2017) 22628-22634.

[27] J. G. Tu, H. P.Lei, Z. J. Yu, S. Q. Jiao, Ordered WO_{3-x} nanorods: facile synthesis and their electrochemical properties for aluminum-ion batteries, Chem. Commun. 54 (2018) 1343-1346.

[28] X. Zhang, G. Zhang, S. Wang, S. Li, S. Jiao, Porous CuO microsphere architectures as high-performance cathode materials for aluminum-ion batteries, J. Mater. Chem. A 6 (2018) 3084-3090.

[29] Z. Li, J. Li, F. Kang, 3D hierarchical AlV_3O_9 microspheres as a cathode material for rechargeable aluminum-ion batteries, Electrochim. Acta 298 (2019) 288-296.

[30] Z. Li, B. Niu, J. Liu, J. Li, F. Kang, Rechargeable Aluminum-Ion Battery Based on MoS_2 Microsphere Cathode, ACS Appl. Mater. Interfaces 10 (2018) 9451-9459.

[31] H. Li, H. Yang, Z. Sun, Y. Shi, H.M. Cheng, F. Li, A highly reversible Co_3S_4 microsphere cathode material for aluminum-ion batteries, Nano Energy 56 (2019) 100-108.

[32] K. Liang, L. Ju, S. Koul, A. Kushima, Y. Yang, Self-Supported Tin Sulfide Porous Films for Flexible Aluminum-Ion Batteries, Adv. Energy Mater. 9 (2019) 1802543.

[33] W. Xing, D. Du, T. Cai, X. Li, J. Zhou, Y. Chai, Q. Xue, Z. Yan, Carbon-encapsulated CoSe nanoparticles derived from metal-organic frameworks as advanced

cathode material for Al-ion battery, J. Power Sources 401 (2018) 6-12.

[34] T. Cai, L. Zhao, H. Hu, T. Li, X. Li, S. Guo, Y. Li, Q. Xue, W. Xing, Z. Yan, L. Wang, Stable $CoSe_2$/carbon nanodice@reduced graphene oxide composites for high-performance rechargeable aluminum-ion batteries, Energy Environ. Sci. 11 (2018) 2341-2347.

[35] J. Tu, H. Lei, M. Wang, Z. Yu, S. Jiao, Facile synthesis of $Ni_{11}(HPO_3)_8(OH)_6$/rGO nanorods with enhanced electrochemical performance for aluminum-ion batteries, Nanoscale 10 (2018) 21284-21291.

[36] H. Lu, Y. Wan, T. Wang, R. Jin, P. Ding, R. Wang, Y. Wang, C. Teng, L. Li, X. Wang, D. Zhou, G. Xue, A high performance SnO_2/C nanocomposite cathode for aluminum-ion batteries, J. Mater. Chem. A 7 (2019) 7213-7220.

[37] G.A. Elia, K. Marquardt, K. Hoeppner, S. Fantini, R. Lin, E. Knipping, W. Peters, J.F. Drillet, S. Passerini, R. Hahn, An Overview and Future Perspectives of Aluminum Batteries, Adv. Mater. 28 (2016) 7564-7579.

[38] X. Tong, F. Zhang, B. Ji, M. Sheng, Y. Tang, Carbon-Coated Porous Aluminum Foil Anode for High-Rate, Long-Term Cycling Stability, and High Energy Density Dual-Ion Batteries, Adv. Mater. 28 (2016) 9979-9985.

[39] X. Tong, F. Zhang, G. Chen, X. Liu, L. Gu, Y. Tang, Core-Shell Aluminum@Carbon Nanospheres for Dual-Ion Batteries with Excellent Cycling Performance under High Rates, Adv. Energy Mater. 8 (2018) 1701967.

[40] G. Zhu, M. Angell, C.J. Pan, M.C. Lin, H. Chen, C.J. Huang, J. Lin, A.J. Achazi, P. Kaghazchi, B.J. Hwang, H. Dai, Rechargeable aluminum batteries: effects of cations

in ionic liquid electrolytes, RSC Adv. 9 (2019) 11322-11330.

[41] C. Xu, S. Zhao, Y. Du, W. Zhang, P. Li, H. Jin, Y. Zhang, Z. Wang, J. Zhang, A High Capacity Aluminum-Ion Battery Based on Imidazole Hydrochloride Electrolyte, ChemElectroChem 6 (2019) 3350-3354.

[42] R. Cang, Y. Song, K. Ye, K. Zhu, J. Yan, J. Yin, G. Wang, D. Cao, Preparation of organic poly material as anode in aqueous aluminum-ion battery, J. Electroanal. Chem. 861 (2020) 113967.

[43] C. Xu, W. Zhang, P. Li, S. Zhao, Y. Du, H. Jin, Y. Zhang, Z. Wang, J. Zhang, High-performance aluminum-ion batteries based on $AlCl_3$/caprolactam electrolytes, Sustain. Energy Fuels, 4 (2020) 121-127.

[44] C. Xu, S. Zhao, Y. Du, Z. Wang, J. Zhang, $AlCl_3$/pyridinium chloride electrolyte-based rechargeable aluminum ion battery, Mater. Lett. 275 (2020) 128040.

[45] Z. Li, B. Niu, Y. Liu, J. Li, F. Kang, Prelithiation treatment of graphite as cathode material for rechargeable aluminum batteries, Electrochim. Acta 263 (2018) 68-75.

[46] Q. Zhang, L. Wang, J. Wang, C. Xing, J. Ge, L. Fan, Z. Liu, X. Lu, M. Wu, X. Yu, H. Zhang, B. Lu, Low-temperature synthesis of edge-rich graphene paper for high-performance aluminum batteries, Energy Storage Mater. 15 (2018) 361-367.

[47] K.L. Ng, T. Dong, J. Anawati, G. Azimi, High-Performance Aluminum Ion Battery Using Cost-Effective $AlCl_3$-Trimethylamine Hydrochloride Ionic Liquid Electrolyte, Adv. Sustainable Syst. 4 (2020) 2000074.

[48] H. Xu, T. Bai, H. Chen, F. Guo, J. Xi, T. Huang, S. Cai, X. Chu, J. Ling, W. Gao, Z. Xu, C. Gao, Low-cost $AlCl_3/Et_3NHCl$ electrolyte for high-performance aluminum-

ion battery, Energy Storage Mater. 17 (2019) 38-45.

[49] H. Huang, F. Zhou, X. Shi, J. Qin, Z. Zhang, X. Bao, Z.-S. Wu, Graphene aerogel derived compact films for ultrafast and high-capacity aluminum ion batteries, Energy Storage Mater. 23 (2019) 664-669.

[50] M. Walter, K.V. Kravchyk, C. Bofer, R. Widmer, M.V. Kovalenko, Polypyrenes as High-Performance Cathode Materials for Aluminum Batteries, Adv. Mater. 30 (2018) e1705644.

[51] X. Zhang, S. Wang, J. Tu, G. Zhang, S. Li, D. Tian, S. Jiao, Flower-like Vanadium Suflide/Reduced Graphene Oxide Composite: An Energy Storage Material for Aluminum-Ion Batteries, ChemSusChem 11 (2018) 709-715.

[52] H. Lahan, S.K. Das, An approach to improve the Al^{3+} ion intercalation in anatase TiO_2 nanoparticle for aqueous aluminum-ion battery, Ionics 24 (2018) 1855-1860.

[53] N. Jayaprakash, S.K. Das, L.A. Archer, The rechargeable aluminum-ion battery, Chem. Commun. 47 (2011) 12610-12612.

[54] M. Morita, T. Shibata, N. Yoshimoto, M. Ishikawa, Anodic behavior of aluminum in organic solutions with different electrolytic salts for lithium ion batteries, Electrochim. Acta 47 (2002) 2787-2793

[55] M. Au, S. McWhorter, H. Ajo, T. Adams, Y. Zhao, J. Gibbs, Free standing aluminum nanostructures as anodes for Li-ion rechargeable batteries, J. Power Sources 195 (2010) 3333-3337.

[56] P.P. Wang, Z. Chen, H. Wang, Z.Y. Ji, Y.P. Feng, J.Q. Wang, J. Liu, M.M. Hu, J.B. Fei, W. Gan, Y. Huang, Energy Storage Mater. 25 (2020) 426.

[57] I.W. Seong, C.H. Hong, B.K. Kim, W.Y. Yoon, The effects of current density and amount of discharge on dendrite formation in the lithium powder anode electrode, J. Power Sources 178 (2008) 769-773.

[58] Y. Yang, S. Liu, C. Chi, J. Hao, J. Zhao, Y. Xu, Y. Li, Electrodeposition of a continuous, dendrite-free aluminum film from an ionic liquid and its electrochemical properties, J. Mater. Sci.-Mater. Electron. 31 (2020) 9937-9945.

[59] S.B. Wang, Q. Ran, R.Q. Yao, H. Shi, Z. Wen, M. Zhao, X.Y. Lang, Q. Jiang, Lamella-nanostructured eutectic zinc-aluminum alloys as reversible and dendrite-free anodes for aqueous rechargeable batteries, Nat. Commun. 11 (2020) 1634.

[60] Y. Long, H. Li, M. Ye, Z. Chen, Z. Wang, Y. Tao, Z. Weng, S.-Z. Qiao, Q.-H. Yang, Suppressing Al dendrite growth towards a long-life Al-metal battery, Energy Storage Mater. 34 (2021) 194-202.

[61] W.J. Cao, J.P. Zheng, Li-ion capacitors with carbon cathode and hard carbon/stabilized lithium metal powder anode electrodes, J. Power Sources 213 (2012) 180-185.

[62] M.S. Park, W.Y. Yoon, Characteristics of a Li/MnO_2 battery using a lithium powder anode at high-rate discharge, J. Power Sources 114 (2003) 237-243.

[63] X.G. Zhang, Fibrous zinc anodes for high power batteries, J. Power Sources 163 (2006) 591-597.

[64] X. Xu, S. Deng, H. Wang, J. Liu, H. Yan, Research Progress in Improving the Cycling Stability of High-Voltage $LiNi_{0.5}Mn_{1.5}O_4$ Cathode in Lithium-Ion Battery, Nano-Micro Lett. 9 (2017) 22.

[65] N. Canever, F.R. Hughson, T. Nann, Solid-Electrolyte Interphases (SEI) in Nonaqueous Aluminum-Ion Batteries, ACS Appl. Energy Mater. 3 (2020) 3673-3683.

[66] Y. Song, S. Jiao, J. Tu, J. Wang, Y. Liu, H. Jiao, X. Mao, Z. Guo, D.J. Fray, A long-life rechargeable Al ion battery based on molten salts, J. Mater. Chem. A 5 (2017) 1282-1291.

[67] N. Zhu, F. Wu, Z. Wang, L. Ling, H. Yang, Y. Gao, S. Guo, l. Suo, H. Li, H. Xu, Y. Bai, C. Wu, Reversible Al^{3+} storage mechanism in anatase TiO_2 cathode material for ionic liquid electrolyte-based aluminum-ion batteries, J. Energy Chem. 51 (2020) 72-80.

[68] Y.T. Kao, S.B. Patil, C.Y. An, S.K. Huang, J.C. Lin, T.S. Lee, Y.C. Lee, H.L. Chou, C.W. Chen, Y.J. Chang, Y.H. Lai, D.Y. Wang, A Quinone-Based Electrode for High-Performance Rechargeable Aluminum-Ion Batteries with a Low-Cost $AlCl_3$/Urea Ionic Liquid Electrolyte, ACS Appl. Mater. Interfaces 12 (2020) 25853-25860.

[69] V.A. Elterman, P.Y. Shevelin, D.L. Chizhov, L.A. Yolshina, E.A. Il'ina, A.V. Borozdin, M.I. Kodess, M.A. Ezhikova, G.L. Rusinov, Development of a novel 1-trifluoroacetyl piperidine-based electrolyte for aluminum ion battery, Electrochim. Acta 323 (2019) 134806.

[70] Y. Park, D. Lee, J. Kim, G. Lee, Y. Tak, Fast charging with high capacity for aluminum rechargeable batteries using organic additive in an ionic liquid electrolyte, Phys. Chem. Chem. Phys. 22 (2020) 27525-27528.

[71] G. Wang, M. Yu, J. Wang, D. Li, D. Tan, M. Loffler, X. Zhuang, K. Mullen, X. Feng, Self-Activating, Capacitive Anion Intercalation Enables High-Power Graphite

Cathodes, Adv. Mater. 30 (2018) e1800533.

[72] A.M. Dimiev, K. Shukhina, N. Behabtu, M. Pasquali, J.M. Tour, Stage Transitions in Graphite Intercalation Compounds: Role of the Graphite Structure, J. Phys. Chem. C 123 (2019) 19246-19253.

[73] J. Wei, W. Chen, D. Chen, K. Yang, An amorphous carbon-graphite composite cathode for long cycle life rechargeable aluminum ion batteries, J. Mater. Sci. Techn. 34 (2018) 983-989.

[74] C. Zhang, R. He, J. Zhang, Y. Hu, Z. Wang, X. Jin, Amorphous Carbon-Derived Nanosheet-Bricked Porous Graphite as High-Performance Cathode for Aluminum-Ion Batteries, ACS Appl. Mater. Interfaces 10 (2018) 26510-26516.

[75] S. Gu, H. Wang, C. Wu, Y. Bai, H. Li, F. Wu, Confirming reversible Al^{3+} storage mechanism through intercalation of Al^{3+} into V_2O_5 nanowires in a rechargeable aluminum battery, Energy Storage Mater. 6 (2017) 9-17.

[76] S. Liu, J.J. Hu, N.F. Yan, G.L. Pan, G.R. Li, X.P. Gao, Aluminum storage behavior of anatase TiO_2 nanotube arrays in aqueous solution for aluminum ion batteries, Energy Environ. Sci. 5 (2012) 9743.

[77] S. Wang, Z. Yu, J. Tu, J. Wang, D. Tian, Y. Liu, S. Jiao, A Novel Aluminum-Ion Battery: Al/$AlCl_3$-[EMIm]Cl/Ni_3S_2@Graphene, Adv. Energy Mater. 6 (2016) 1600137.

[78] Y. Hu, B. Luo, D. Ye, X. Zhu, M. Lyu, L. Wang, An Innovative Freeze-Dried Reduced Graphene Oxide Supported SnS_2 Cathode Active Material for Aluminum-Ion Batteries, Adv. Mater. 29 (2017) 1606132.

[79] L. Geng, G. Lv, X. Xing, J. Guo, Reversible Electrochemical Intercalation of

Aluminum in Mo_6S_8, Chem. Mater. 27 (2015) 4926-4929.

[80] D. Kim, S.H. Kang, M. Slater, S. Rood, J.T. Vaughey, N. Karan, M. Balasubramanian, C.S. Johnson, Enabling Sodium Batteries Using Lithium-Substituted Sodium Layered Transition Metal Oxide Cathodes, Adv. Energy Mater. 1 (2011) 333-336.

[81] F. Nacimiento, M. Cabello, R. Alcántara, C. Pérez-Vicente, P. Lavela, J.L. Tirado, Exploring an Aluminum Ion Battery Based on Molybdite as Working Electrode and Ionic Liquid as Electrolyte, J. Electrochem. Soc. 165 (2018) A2994-A2999.

[82] J.M. Wu, Z.Z. Li, Nanostructured composite obtained by mechanically driven reduction reaction of CuO and Al powder mixture, J. Alloy. Compd. 299 (2000) 9-16.

[83] X. Zhang, X. Xu, W. He, G. Yang, J. Shen, J. Liu, Q. Liu, $LiFePO_4/NaFe_3V_9O_{19}$/porous glass nanocomposite cathodes for Li^+/Na^+ mixed-ion batteries, J. Mater. Chem. A 3 (2015) 22247-22257.

[84] X. Yu, B. Wang, D. Gong, Z. Xu, B. Lu, Graphene Nanoribbons on Highly Porous 3D Graphene for High-Capacity and Ultrastable Al-Ion Batteries, Adv. Mater. 29 (2017) 1604118.

[85] S.J. Deng, H. Zhu, G.Z. Wang, M. Luo, S.H. Shen, C.Z. Ai, L. Yang, S.W. Lin, Q.H. Zhang, L. Gu, B. Liu, Y. Zhang, Q. Liu, G.X. Pan, Q.Q. Xiong, X.L. Wang, X.H. Xia, J.P. Tu, Boosting fast energy storage by synergistic engineering of carbon and deficiency, Nat. Commun. 11 (2020) 132.

[86] P. Bhauriyal, A. Mahata, B. Pathak, The staging mechanism of $AlCl_4$ intercalation in a graphite electrode for an aluminium-ion battery, Phys. Chem. Chem. Phys. 19

(2017) 7980-7989.

[87] H. Chen, C. Chen, Y. Liu, X. Zhao, N. Ananth, B. Zheng, L. Peng, T. Huang, W. Gao, C. Gao, High-Quality Graphene Microflower Design for High-Performance Li-S and Al-Ion Batteries, Adv. Energy Mater. 7 (2017) 1700051.

[88] X.D. Huang, Y. Liu, H.W. Zhang, J. Zhang, O. Noonan, C. Z. Yu, Free-standing Monolithic Nanoporous Graphene Foam as High Performance Aluminum-ion Battery Cathode, J. Mater. Chem. A 5 (2017) 19416-19421.

[89] L. Kong, J. Zhu, W. Shuang, X.H. Bu, Nitrogen-Doped Wrinkled Carbon Foils Derived from MOF Nanosheets for Superior Sodium Storage, Adv. Energy Mater. 8 (2018) 1801515.

[90] L. Kong, Q. Chen, X. Shen, Z. Xu, C. Xu, Z. Ji, J. Zhu, MOF derived nitrogen-doped carbon polyhedrons decorated on graphitic carbon nitride sheets with enhanced electrochemical capacitive energy storage performance, Electrochim. Acta 265 (2018) 651-661.

[91] J. Zhang, J. Fang, J. Han, T. Yan, L. Shi, D. Zhang, N, P, S co-doped hollow carbon polyhedra derived from MOF-based core–shell nanocomposites for capacitive deionization, J. Mater. Chem. A 6 (2018) 15245-15252.

[92] Z.L. Yu, G.C. Li, N. Fechler, N. Yang, Z.Y. Ma, X. Wang, M. Antonietti, S.H. Yu, Polymerization under Hypersaline Conditions: A Robust Route to Phenolic Polymer-Derived Carbon Aerogels, Angew. Chem. 55 (2016) 14623-14627.

[93] B. Lv, P. Li, Y. Liu, S. Lin, B. Gao, B. Lin, Nitrogen and phosphorus co-doped carbon hollow spheres derived from polypyrrole for high-performance supercapacitor

electrodes, Appl. Surface Sci. 437 (2018) 169-175.

[94] Y. Zhang, T.T. Qu, K. Xiang, Y. Shen, S.Y. Chen, M.J. Xie, X.F. Guo, In-situ formation/carbonization of quinone-amine polymers towards hierarchical-pore carbon foam with high faradaic activity for energy storage, J. Mater. Chem. A 6 (2018) 2353-2359.

[95] J.S.M. Lee, M.E. Briggs, C.C. Hu, A.I. Cooper, Controlling electric double-layer capacitance and pseudocapacitance in heteroatom-doped carbons derived from hypercrosslinked microporous polymers, Nano Energy 46 (2018) 277-289.

[96] A.B. Deshmukh, A.C. Nalawade, I. Karbhal, M.S. Qureshi, M.V. Shelke, Electrochemical capacitive energy storage in PolyHIPE derived nitrogen enriched hierarchical porous carbon nanosheets, Carbon 128 (2018) 287-295.

[97] M. Nagalakshmi, N. Kalaiselvi, Mesoporous dominant cashewnut sheath derived bio-carbon anode for LIBs and SIBs, Electrochim. Acta 304 (2019) 175-183.

[98] X. Yang, Z. Jiang, B. Fei, J. Ma, X. Liu, Graphene functionalized bio-carbon xerogel for achieving high-rate and high-stability supercapacitors, Electrochim. Acta, 282 (2018) 813-821.

[99] M. Demir, A.A. Farghaly, M.J. Decuir, M.M. Collinson, R.B. Gupta, Supercapacitance and oxygen reduction characteristics of sulfur self-doped micro/mesoporous bio-carbon derived from lignin, Mater. Chem. Phys. 216 (2018) 508-516.

[100] M. Vadivazhagan, P. Parameswaran, U. Mani, K. Nallathamby, Waste-Driven Bio-Carbon Electrode Material for Na-Ion Storage Applications, ACS Sustainable

Chem. Eng. 6 (2018) 13915–13923.

[101] Z. Wang, S. Yun, X. Wang, C. Wang, Y. Si, Y. Zhang, H. Xu, Aloe peel-derived honeycomb-like bio-based carbon with controllable morphology and its superior electrochemical properties for new energy devices, Ceramics International, 45 (2019) 4208-4218.

[102] B.H. Shan, Y.P. Cui, W. Liu, Y. Zhang, S. Liu, H.L. Wang, L.J. Sun, Z.P. Wang, R.T. Wu, Fibrous Bio-Carbon Foams: A New Material for Lithium-Ion Hybrid Supercapacitors with Ultrahigh Integrated Energy/Power Density and Ultralong Cycle Life, ACS Sustainable Chem. Eng. 6 (2018) 14989-15000.

[103] R.R. Salunkhe, J. Tang, N. Kobayashi, J. Kim, Y. Ide, S. Tominaka, J.H. Kim, Y. Yamauchi, Ultrahigh performance supercapacitors utilizing core-shell nanoarchitectures from a metal-organic framework-derived nanoporous carbon and a conducting polymer, Chem. Sci. 7 (2016) 5704-5713.

[104] C. Wang, Y.V. Kaneti, Y. Bando, J. Lin, C. Liu, J. Li, Y. Yamauchi, Metal–organic framework-derived one-dimensional porous or hollow carbon-based nanofibers for energy storage and conversion, Mater. Horiz. 5 (2018) 394-407.

[105] X. Ma, L. Li, R. Chen, C. Wang, H. Li, S. Wang, Heteroatom-doped nanoporous carbon derived from MOF-5 for CO_2 capture, Appl. Surface Sci. 435 (2018) 494-502.

[106] I.T. Kim, S. Shin, M.W. Shin, Development of 3D interconnected carbon materials derived from Zn-MOF-74@carbon nanofiber web as an efficient metal-free electrocatalyst for oxygen reduction, Carbon 135 (2018) 35-43.

[107] Z. Tang, G. Zhang, H. Zhang, L. Wang, H. Shi, D. Wei, H. Duan, MOF-derived

N-doped carbon bubbles on carbon tube arrays for flexible high-rate supercapacitors, Energy Storage Mater. 10 (2018) 75-84.

[108] W. Yang, X. Li, Y. Li, R. Zhu, H. Pang, Applications of Metal-Organic-Framework-Derived Carbon Materials, Adv. Mater. 31 (2019) e1804740.

[109] L. Chai, L. Zhang, X. Wang, L. Xu, C. Han, T.-T. Li, Y. Hu, J. Qian, S. Huang, Bottom-up synthesis of MOF-derived hollow N-doped carbon materials for enhanced ORR performance, Carbon 146 (2019) 248-256.

[110] K.Y. Zou, Z.X. Li, Controllable Syntheses of MOF-Derived Materials, Chem. 24 (2018) 6506-6518.

[111] M.L. Yue, C.Y. Yu, H.H. Duan, B.L. Yang, X.X. Meng, Z.X. Li, Six Isomorphous Window-Beam MOFs: Explore the Effects of Metal Ions on MOF-Derived Carbon for Supercapacitors, Chem. 24 (2018) 16160-16169.

[112] X. Xu, H. Wang, Y. Xie, J. Liu, H. Yan, W. Liu, Graphitized Mesoporous Carbon Derived from ZIF-8 for Suppressing Sulfation in Lead Acid Battery and Dendritic Lithium Formation in Lithium Ion Battery, J. Electrochem. Soc. 165 (2018) A2978-A2984.

[113] X. Xu, C. Qi, Z. Hao, H. Wang, J. Jiu, J. Liu, H. Yan, K. Suganuma, The Surface Coating of Commercial $LiFePO_4$ by Utilizing ZIF-8 for High Electrochemical Performance Lithium Ion Battery, Nano-Micro Lett. 10 (2018) 1.

[114] X. Xu, Z. Hao, H. Wang, J. Liu, H. Yan, Mesoporous carbon derived from ZIF-8 for improving electrochemical performances of commercial $LiFePO_4$, Mater. Lett. 197 (2017) 209-212.

[115] X. Xu, Z. Hao, H. Wang, C. Hu, J. Liu, Y. Jin, In-situ preparation of mesoporous carbon contained graphite-zinc quantum dots for enhancing the electrochemical performance of $LiFePO_4$, Ionics 25 (2018) 89-98.

[116] Y. Su, Z. Yao, F. Zhang, H. Wang, Z. Mics, E. Cánovas, M. Bonn, X. Zhuang, X. Feng, Sulfur-Enriched Conjugated Polymer Nanosheet Derived Sulfur and Nitrogen co-Doped Porous Carbon Nanosheets as Electrocatalysts for Oxygen Reduction Reaction and Zinc-Air Battery, Adv. Function. Mater. 26 (2016) 5893-5902.

[117] M. Kopeć, M. Lamson, R. Yuan, C. Tang, M. Kruk, M. Zhong, K. Matyjaszewski, T. Kowalewski, Polyacrylonitrile-derived nanostructured carbon materials, Progress in Polymer Science, 92 (2019) 89-134.

[118] S. Dutta, A. Bhaumik, K.C.W. Wu, Hierarchically porous carbon derived from polymers and biomass: effect of interconnected pores on energy applications, Energy Environ. Sci. 7 (2014) 3574-3592.

[119] Q. Zhao, P.Y. Chen, S.K. Li, X.T. Liu, L.A. Archer, Solid-state Polymer Electrolytes Stabilized by Task-specific Salt Additives, J. Mater. Chem. A 7 (2019) 7823.

[120] L. Shao, M. Liu, J. Huang, Y.N. Liu, CO_2 capture by nitrogen-doped porous carbons derived from nitrogen-containing hyper-cross-linked polymers, J. Colloid Interf. Sci. 513 (2018) 304-313.

[121] Y.T. Tan, Y.S. Liu, Y.F. Zhang, C.G. Xu, L.B. Kong, L. Kang, F. Ran, Dulse-derived porous carbon–polyaniline nanocomposite electrode for high-performance supercapacitors, J. Appl. Polym. Sci. 135 (2018) 45776.

[122] X. Li, T. Wang, P. Duan, M. Baldini, H.T. Huang, B. Chen, S.J. Juhl, D. Koeplinger, V.H. Crespi, K. Schmidt-Rohr, R. Hoffmann, N. Alem, M. Guthrie, X. Zhang, J.V. Badding, Carbon Nitride Nanothread Crystals Derived from Pyridine, J. Am. Chem. Soc. 140 (2018) 4969-4972.

[123] R.T. Woodward, F. Markoulidis, F. De Luca, D.B. Anthony, D. Malko, T.O. McDonald, M.S.P. Shaffer, A. Bismarck, Carbon foams from emulsion-templated reduced graphene oxide polymer composites: electrodes for supercapacitor devices, J. Mater. Chem. A 6 (2018) 1840-1849.

[124] D.R. Lu, C.M. Xiao, S.J. Xu, Starch-based completely biodegradable polymer materials, Express Polym. Lett. 3 (2009) 366-375.

[125] R. Taherian, M. J. Hadianfard, A. N. Golikand, Manufacture of a polymer-based carbon nanocomposite as bipolar plate of proton exchange membrane fuel cells, Mater. Design 49 (2013) 242-251.

[126] M. Santhiago, P.S. Garcia, M. Strauss, Bio-based nanostructured carbons toward sustainable technologies, Curr. Opin. Green Sustain. Chem. 12 (2018) 22-26.

[127] S. Sathyamoorthi, N. Phattharasupakun, M. Sawangphruk, Environmentally benign non-fluoro deep eutectic solvent and free-standing rice husk-derived bio-carbon based high-temperature supercapacitors, Electrochim. Acta 286 (2018) 148-157.

[128] K. Mensah-Darkwa, C. Zequine, P. Kahol, R. Gupta, Supercapacitor Energy Storage Device Using Biowastes: A Sustainable Approach to Green Energy, Sustainability 11 (2019) 414.

[129] S. Arnold, A. Rodriguez-Uribe, M. Misra, A.K. Mohanty, Slow pyrolysis of bio-

oil and studies on chemical and physical properties of the resulting new bio-carbon, J. Clean. Prod. 172 (2018) 2748-2758.

[130] W. J. Liu, H. Jiang and H. Q. Yu, Emerging applications of biochar-based materials for energy storage and conversion, Energy Environ. Sci. 12 (2019) 1751-1779.

[131] L. Jiang, L. Sheng, Z. Fan, Biomass-derived carbon materials with structural diversities and their applications in energy storage, Sci. China Mater. 61 (2017) 133-158.

[132] C. Xia, J. Guo, Y. Lei, H. Liang, C. Zhao, H.N. Alshareef, Rechargeable Aqueous Zinc-Ion Battery Based on Porous Framework Zinc Pyrovanadate Intercalation Cathode, Adv. Mater. 30 (2018) 1705580.

[133] X. Shen, T. Sun, L. Yang, A. Krasnoslobodtsev, R. Sabirianov, M. Sealy, W.N. Mei, Z. Wu, L. Tan, Ultra-fast charging in aluminum-ion batteries: electric double layers on active anode, Nat. Commun. 12 (2021) 820.

[134] Q. Peng, B. Yang, L. Liu, C. Song, B. Friedrich, Porous TiAl alloys fabricated by sintering of TiH_2 and Al powder mixtures, J. Alloy. Compd. 656 (2016) 530-538.

[135] D. Singh, A. Mittal, V. Jain, D. Gupta, V.K. Singla, Investigations on Fabrication Techniques of Aluminium-Based Porous Material, Advances in Manufacturing Processes 1 (2019) 219-227.

[136] X. Xu, S. Wang, H. Wang, B. Xu, C. Hu, Y. Jin, J. Liu, H. Yan, The suppression of lithium dendrite growth in lithium sulfur batteries: A review, J. Energy Storage 13 (2017) 387-400.

[137] J. Shim, J.W. Lee, K.Y. Bae, H.J. Kim, W.Y. Yoon, J.C. Lee, Dendrite

Suppression by Synergistic Combination of Solid Polymer Electrolyte Crosslinked with Natural Terpenes and Lithium-Powder Anode for Lithium-Metal Batteries, ChemSusChem 10 (2017) 2274-2283.

[138] X. Xu, J. Liu, Q. Zhang, H. Wang, A facile approach to suppress the sulfation in lead acid batteries using N-doped carbon derived from chitosan, Mater. Lett. 247 (2019) 29-31.

[139] X. Xu, Z. Hao, H. Wang, Y. Xie, J. Liu, H. Yan, A facile synthetic route of nitrogen-doped graphite derived from chitosan for modifying $LiFePO_4$ cathode, J. Mater. Sci.-Mater. Electron. 29 (2018) 16630-16638.

[140] C.S. Yan, C.D. Lv, L.G. Wang, W. Cui, L.Y. Zhang, K.N. Dinh, H.T. Tan, C. Wu, T.P. Wu, Y. Ren, J.Q. Chen, Z. Liu, M. Srinivasan, X.H. Rui, Q.Y. Yan, G.H. Yu, Architecting a Stable High-Energy Aqueous Al-Ion Battery, J. Am. Chem. Soc. 142 (2020) 15295-15304.

[141] L. Xiang, X.W. Ou, X.Y. Wang, Z.M. Zhou, X, Li, Y.B. Tang, Highly Concentrated Electrolyte towards Enhanced Energy Density and Cycling Life of Dual-Ion Battery, Angew. Chem. Int. Ed. 59 (2020) 17924-17930.

[142] Q. Pan, D. Gong, Y. Tang, Recent progress and perspective on electrolytes for sodium/potassium-based devices, Energy Storage Mater. 31 (2020) 328-343.

[143] J.Y. Hwang, S.T. Myung, Y.K. Sun, Sodium-ion batteries: present and future, Chem. Soc. Rev. 46 (2017) 3529-3614.

[144] H. Yaghoobnejad Asl, J. Fu, H. Kumar, S.S. Welborn, V.B. Shenoy, E. Detsi, In Situ Dealloying of Bulk Mg_2Sn in Mg-Ion Half Cell as an Effective Route to

Nanostructured Sn for High Performance Mg-Ion Battery Anodes, Chem. Mater. 30 (2018) 1815-1824.

[145] M. Wang, C. Jiang, S. Zhang, X. Song, Y. Tang, H.M. Cheng, Reversible calcium alloying enables a practical room-temperature rechargeable calcium-ion battery with a high discharge voltage, Nat. Chem. 10 (2018) 667-672.

[146] B. Ji, H. He, W. Yao, Y. Tang, Recent Advances and Perspectives on Calcium-Ion Storage: Key Materials and Devices, Adv. Mater. 33 (2021) e2005501.

[147] J. Wang, C.W. Sun, Y.D. Gong, H.R. Zhang, J.A. Alonso, M.T. María Teresa Fernández-Díaz, Z. L. Wang, J. B. Goodenough, Imaging the diffusion pathway of Al^{3+} ion in NASICON-type $(Al_{0.2}Zr_{0.8})_{20/19}Nb(PO_4)_3$ as electrolyte for rechargeable solid-state Al batteries, Chin. Phys. B 27 (2018) 128201.

Photograph and biography of authors:

Xiaolong Xu obtained his Ph.D. degree in Materials Science and Engineering of the Beijing University of Technology in 2020. Now he is an Associate Professor at School of Materials Science and Engineering in Qilu University of Technology (Shandong Academy of Sciences). He is major in the electrochemical energy storage materials and devices, mainly including metal-organic frameworks, battery materials, carbon materials, metal-air batteries, metal-ion batteries and lead-acid batteries, ect..

Kwan San Hui obtained a Ph.D. degree in Mechanical Engineering of the Hong Kong University of Science and Technology in 2008. He is a Reader in Mechanical Engineering at School of Engineering of University of East Anglia, UK. He has extensive research experience in material science, catalysis, air/water pollution control, and energy storage.

Kwun Nam Hui obtained his PhD degree in Electrical and Electronic Engineering of the University of Hong Kong in 2009. He is an Associate Professor at the Institute of Applied Physics and Materials Engineering of the University of Macau. His current research focuses on the design and synthesis of nanostructured materials for electrochemical energy storage and conversion including batteries, supercapacitors, and fuel cells.

Highlights

1. We reported the challenges, outlooks and potential research directions for AIBs.
2. Challenges/outlooks involve anode design, electrolyte exploitation, cathode selection.
3. Research directions focus on sustainable, low-cost, and high-power density AIBs.
4. Acquisition of green and low-cost carbonaceous cathode materials is highlighted.